frontiers | Frontiers in Endocrinology

TYPE Original Research
PUBLISHED 04 December 2023
DOI 10.3389/fendo.2023.1266527

OPEN ACCESS

EDITED BY
Elzbieta Janda,
Magna Græcia University, Italy

REVIEWED BY
Davide Gnocchi,
University of Bari Aldo Moro, Italy
Pankaj Yadav,
SASTRA University, India

*CORRESPONDENCE
Frances M. Sladek
Frances.sladek@ucr.edu

†PRESENT ADDRESSES
Jonathan R. Deans,
OccamzRazor, Johnson &Johnson Innovation Labs, New York, NY, United States
Linh M. Vuong,
Department of Biological Chemistry, School of Medicine, University of California, Irvine, CA, United States
Johannes Fahrmann,
Department of Clinical Cancer Prevention, University of Texas MD Anderson Cancer Center, Houston, TX, United States

‡These authors have contributed equally to this work

RECEIVED 25 July 2023
ACCEPTED 06 November 2023
PUBLISHED 04 December 2023

CITATION
Deans JR, Deol P, Titova N, Radi SH, Vuong LM, Evans JR, Pan S, Fahrmann J, Yang J, Hammock BD, Fiehn O, Fekry B, Eckel-Mahan K and Sladek FM (2023) HNF4α isoforms regulate the circadian balance between carbohydrate and lipid metabolism in the liver.
Front. Endocrinol. 14:1266527.
doi: 10.3389/fendo.2023.1266527

HNF4α isoforms regulate the circadian balance between carbohydrate and lipid metabolism in the liver

Jonathan R. Deans[1,2†], Poonamjot Deol[1‡], Nina Titova[1‡], Sarah H. Radi[1,3‡], Linh M. Vuong[1†‡], Jane R. Evans[1], Songqin Pan[4], Johannes Fahrmann[5†], Jun Yang[6], Bruce D. Hammock[6], Oliver Fiehn[5], Baharan Fekry[7], Kristin Eckel-Mahan[7,8] and Frances M. Sladek[1*]

[1]Department of Molecular, Cell and Systems Biology, University of California, Riverside, Riverside, CA, United States, [2]Genetics, Genomics and Bioinformatics Graduate Program, University of California, Riverside, Riverside, CA, United States, [3]Biochemistry and Molecular Biology Graduate Program, University of California, Riverside, Riverside, CA, United States, [4]Proteomics Core, Institute for Integrative Genome Biology, University of California, Riverside, Riverside, CA, United States, [5]National Institutes of Health West Coast Metabolomics Center, University of California, Davis, Davis, CA, United States, [6]Department of Entomology and Nematology & UCD Comprehensive Cancer Center, University of California, Davis, Davis, CA, United States, [7]Department of Biochemistry and Molecular Biology, McGovern Medical School at the University of Texas Health Science Center (UT Health), Houston, TX, United States, [8]Institute of Molecular Medicine, McGovern Medical School at the University of Texas Health Science Center (UT Health), Houston, TX, United States

Hepatocyte Nuclear Factor 4α (HNF4α), a master regulator of hepatocyte differentiation, is regulated by two promoters (P1 and P2) which drive the expression of different isoforms. P1-HNF4α is the major isoform in the adult liver while P2-HNF4α is thought to be expressed only in fetal liver and liver cancer. Here, we show that P2-HNF4α is indeed expressed in the normal adult liver at Zeitgeber time (ZT)9 and ZT21. Using exon swap mice that express only P2-HNF4α we show that this isoform orchestrates a distinct transcriptome and metabolome via unique chromatin and protein-protein interactions, including with different clock proteins at different times of the day leading to subtle differences in circadian gene regulation. Furthermore, deletion of the *Clock* gene alters the circadian oscillation of P2- (but not P1-)HNF4α RNA, revealing a complex feedback loop between the HNF4α isoforms and the hepatic clock. Finally, we demonstrate that while P1-HNF4α drives gluconeogenesis, P2-HNF4α drives ketogenesis and is required for elevated levels of ketone bodies in female mice. Taken together, we propose that the highly conserved two-promoter structure of the *Hnf4a* gene is an evolutionarily conserved mechanism to maintain the balance between gluconeogenesis and ketogenesis in the liver in a circadian fashion.

KEYWORDS

cytochrome P450, metabolic switch, sex-specific gene expression, fasting, circadian clock, ketogenesis, alternative promoter, nuclear receptor

Introduction

Roughly 30% of human genes contain alternative promoters and yet the functional significance of the majority of those promoters, and the transcripts they generate, is woefully understudied. One such gene is the nuclear receptor (NR) Hepatocyte Nuclear Factor 4 alpha (HNF4α), a liver-enriched transcription factor (TF) best known as a master regulator of liver-specific gene expression and mutated in Maturity Onset Diabetes of the Young 1 (MODY1) (1, 2). In mice, HNF4α is essential for fetal liver function (3) and liver knockout (KO) mice die within six weeks of birth with a fatty liver (4).

The human *HNF4A* and mouse *Hnf4a* genes are highly conserved and regulated by proximal P1 and distal P2 promoters. P1 drives the expression of transcripts containing exon 1A while P2 transcripts contain exon 1D, resulting in a loss of the N-terminal activation function 1 (AF-1). In the adult liver P1 is presumed to be the only active promoter, while during fetal liver development both P1 and P2 are active (5, 6). The first P2-HNF4α transcript cloned, HNF4α7, was from the embryonal carcinoma cell line F9 (7), suggesting that it might play a role in cancer as well as fetal development. P1-HNF4α is downregulated in liver cancer and acts as a tumor suppressor (8–12), while overexpression of P2-HNF4α is linked to poor prognosis in hepatocellular carcinoma (HCC) (13).

The circadian clock regulates all aspects of physiology, including lipid metabolism. The liver is a major driver of the peripheral clock which is entrained by feeding and plays a role in fatty liver disease as well as hormonal homeostasis (14–19). While P2-HNF4α is not typically found in normal adult liver, it is expressed under certain stress conditions that involve metabolic adaptation by cells, such as cancer and high fat diet (HFD) feeding (12, 20). Furthermore, both cancer and HFD-induced obesity are known to be exacerbated by disruption of circadian rhythms (21, 22). Since HNF4α is a known driver of liver metabolism and has been shown to play a role in hepatic circadian rhythms (2), we hypothesized that P2-HNF4α may play a unique role in liver metabolism and may intersect with the circadian clock.

To address the physiological role of P2-HNF4α, we employed exon swap mice (α7HMZ), which substitute exon 1A with exon 1D in the P1 promoter and demonstrate a role for the AF-1 domain *in vivo* (23). We compared the α7HMZ adult mice (express only P2-HNF4α) to wildtype (WT) mice (express P1-HNF4α) using RNA-seq, ChIP-seq, rapid immunoprecipitation mass spectrometry of endogenous proteins (RIME), protein binding microarrays (PBMs) and metabolomics. An orchestrated, altered hepatic transcriptome in P2-HNF4α livers reveals large, significant differences in several cytochrome P450 transcripts and small but significant differences in key clock regulators, as well as expression of female-specific genes in the male livers. The distinct P2-HNF4α transcriptome appears to be due to altered protein-protein interactions, as well as altered chromatin binding but not differences in innate DNA binding specificity. Expression of P2-HNF4α is observed at Zeitgeber time (ZT) 9 and ZT21 in WT adult livers, and is upregulated in *Clock*-deficient mice. The P2-HNF4α hepatic metabolome is enriched in lipids and ketone bodies while mice expressing only P1-HNF4α exhibit enhanced gluconeogenesis and lack the elevated levels of ketone bodies normally found in females (24). Given that the P1/P2 promoter structure of the *Hnf4a* gene and many of its target genes are conserved across more than 90 million years (2, 25), our results suggest that expression of P2-HNF4α in the liver is an evolutionarily conserved mechanism to balance carbohydrate and fatty acid metabolism during the circadian cycle.

Results

The P2-HNF4α transcriptome has neither a fetal nor a cancer profile

Exon swap α7HMZ mice were verified to express P2-HNF4α, but not P1-HNF4α, RNA and protein in adult liver (Figures 1A–C). RNA-seq of adult male livers revealed a significant difference (padj ≤ 0.01) in ~1600 genes between WT and α7HMZ, both up- (831) and downregulated (792) in α7HMZ (Figure 1D). The most downregulated (e.g., *Scnn1a, Cyp2c50, Rdh16f2, Ces2e*) and upregulated genes (e.g., *Rad51b, Pcp4l1, Cyp2b13, Cyp2b9*) exhibited nearly 30-fold effects (Figure 1E). Kegg pathway analysis revealed discrete metabolic pathways upregulated in α7HMZ versus WT livers (e.g., oxidative phosphorylation and non-alcoholic fatty liver disease), suggesting a purposeful alteration in gene expression (Figure 1F). For example, cell adhesion molecules, drug and linoleic acid metabolism and steroid hormone biosynthesis genes were enriched in WT mice while the ribosome, oxidative phosphorylation and RNA transport and processing were enriched in α7HMZ. Several disease pathways were also enriched among the P2-specific genes, including non-alcoholic fatty liver disease (NAFLD), viral carcinogenesis, alcoholism and neurological diseases (Parkinson's, Huntington's, Alzheimer's) (Figure 1F). Comparison of α7HMZ versus WT differentially expressed genes (DEGs) with HNF4α liver KO expression data (26) revealed that ~100 of the WT-specific genes (but none of the α7HMZ-specific genes) were downregulated in the HNF4α KO (Supplementary Figure 1A), confirming P1-HNF4α predominance in the adult liver.

The α7HMZ versus WT DEGs were compared with adult versus fetal (E14.5) liver DEGs (Figure 1G). More than two thirds of the genes upregulated in WT livers were also upregulated in the adult liver, while ~10% were enriched in fetal livers (562 versus 87, respectively). In contrast, α7HMZ-upregulated genes were more evenly split between adult and fetal liver (Figure 1G). Interestingly, alpha-fetoprotein (*Afp*) and other fetal liver genes were expressed at a lower level in α7HMZ (Supplementary Figure 1B), suggesting that the α7HMZ "program" is not simply a fetal one. Furthermore, while α7HMZ mice have a significantly ($p < 0.01$) higher liver-to-body weight ratio than WT or α1HMZ (exon 1A swapped for exon 1D in the P2 promoter) at postnatal day 14, the reverse (α1HMZ > α7HMZ) is observed at

10.3389/fendo.2023.1266527

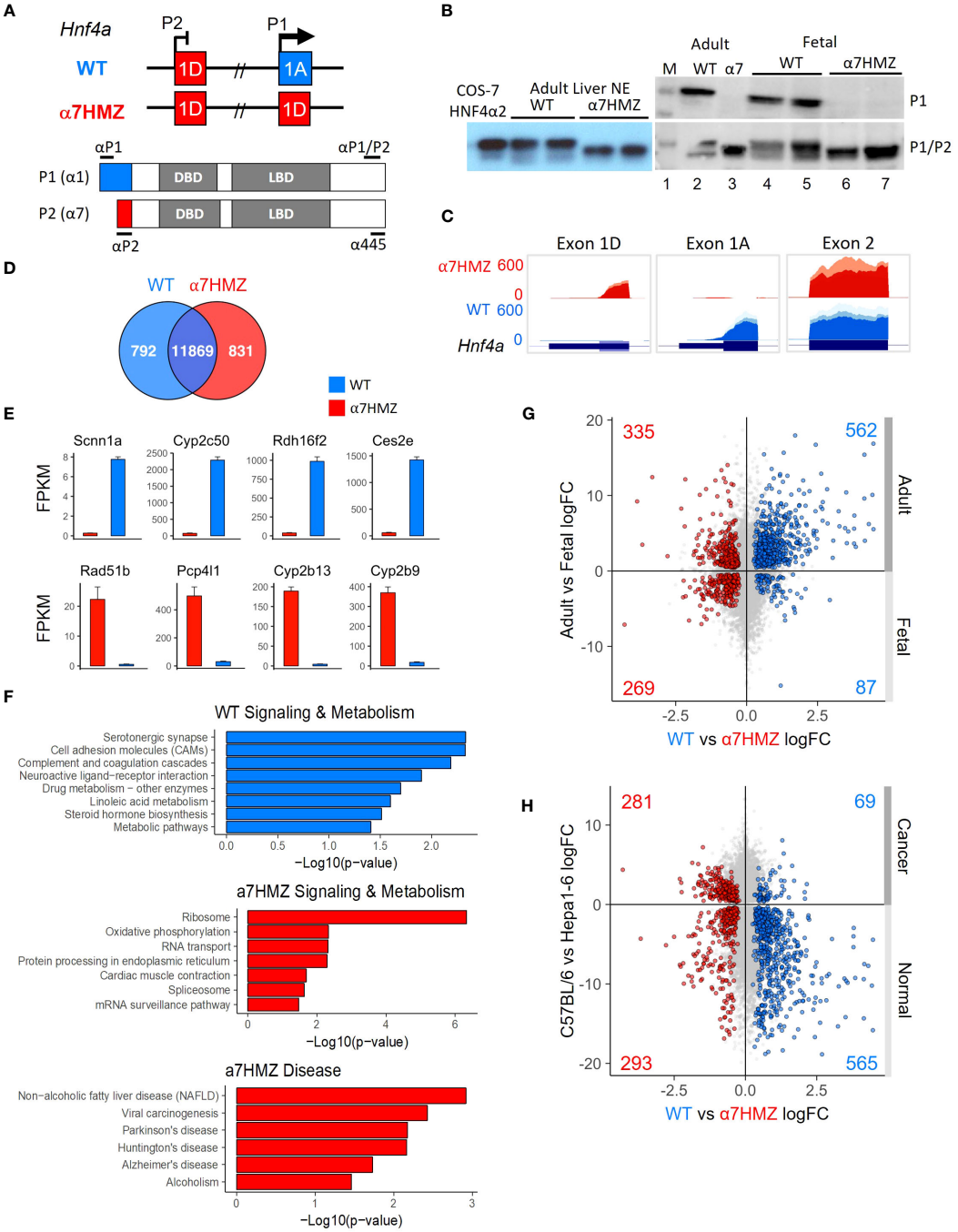

FIGURE 1
P2-HNF4α correlates with neither a fetal nor a cancer profile. **(A)** *Hnf4a* P1 and P2 promoters and first exons in WT and α7HMZ mice, protein products (P1: HNF4α1; P2: HNF4α7) and epitopes for P1-, P2-specific and P1/P2-common antibodies (Abs). DBD, DNA binding domain; LBD, ligand binding domain. **(B)** Immunoblots (IBs) of nuclear (NE) and whole cell liver extracts (WCE) with P1-specific and P1/P2-HNF4α Abs. M, molecular weight markers (top band, 54 kD). COS-7 α2, NE of cells transfected with human HNFα2. **(C)** UCSC Genome Browser view of liver RNA-seq reads mapping to *Hnf4a in mm10*. Exon 1D: chr2:163,506,818-163,507,018; Exon 1A: chr2:163,547,117-163,547,445; Exon 2: ch2: 163,551,501-163,551,803. **(D)** Number of common and significantly (padj ≤ 0.01) dysregulated genes in WT and α7HMZ male liver RNA-seq (10:30 AM, ZT3.5) with baseMean ≥ 10 (n=3). **(E)** Average FPKM of most significantly up- and downregulated genes in α7HMZ livers compared to WT. All, padj <0.01. **(F)** Enriched KEGG pathways for WT- and α7HMZ-uniquely expressed genes. **(G)** RNA-seq log2 fold-change (log2FC) values between WT and α7HMZ, plotted against adult and E14.5 fetal mouse livers from ENCODE. Colored data points (total number noted in each quadrant), padj ≤ 0.01 in both datasets: blue, up in WT; red, up in α7HMZ. **(H)** As in **(G)** except plotted versus data from murine hepatoma cell line (Hepa1-6) and WT C57BL/6 livers. See Supplementary Tables 1, 2 for full lists of genes and Supplementary Figure 1 for additional comparisons.

10.3389/fendo.2023.1266527

postnatal day 21 (Supplementary Figure 1C). Finally, proliferation genes *Mki67* and *Pcna* were not upregulated in α7HMZ adult livers as one might anticipate for a predominantly fetal transcription factor (TF) (Supplementary Figure 1E).

To determine whether α7HMZ livers exhibit a cancer profile, the α7HMZ versus WT DEGs were plotted against DEGs of normal C57BL/6 livers versus murine hepatoma cell line Hepa1-6 (Figure 1H). As anticipated, genes upregulated in the WT liver were preferentially expressed at higher levels in normal liver compared to liver cancer (565 versus 69, respectively). In contrast, genes more highly expressed in α7HMZ livers were not enriched in liver cancer (Figure 1H and Supplementary Figure 1D). Taken together, these results indicate that P2-HNF4α drives a specific program of gene expression in the adult liver distinct from that of P1-HNF4α that is neither completely fetal- nor cancer-like, suggesting an alternative role for P2-HNF4α.

P2-HNF4α livers are less sensitive to the circadian clock

Since NRs are known to play an important role in regulating the circadian clock in the liver and HNF4α has been shown to play a role in hepatic circadian rhythms (27–30), RNA-seq of WT and α7HMZ livers was performed at three different time points (10:30, 13:30, 20:30, equivalent to ZT3.5, ZT6.5 and ZT13.5, respectively). While the expression of ~250 to 500 genes was significantly altered (padj <0.01, absolute log2FC ≥ 1) between any two of the time points in WT mice, less than half that number was altered in α7HMZ livers (Figure 2A, *top*), suggesting a reduced sensitivity of α7HMZ livers to the circadian clock. There were also more genes down- than upregulated in α7HMZ livers (Figure 2A, *bottom*), consistent with the loss of AF-1 function *in vitro* (7, 31). A volcano plot of DEGs highlights differential gene expression between WT and α7HMZ

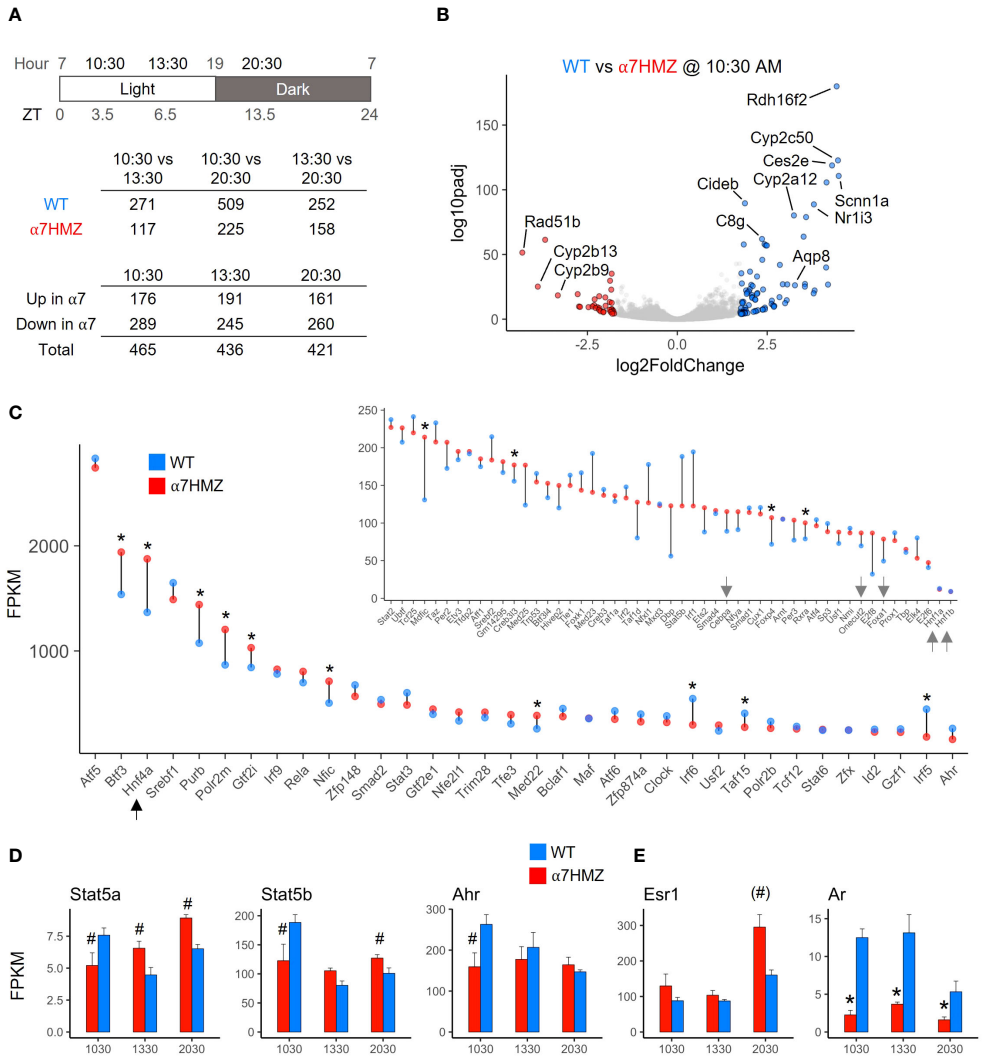

FIGURE 2
HNF4α is one of the most highly expressed TFs in the liver; P2-HNF4α promotes "feminization" of the mouse liver. **(A)** Number of genes with significant gene expression changes (padj ≤ 0.01, log2FC ≥ 1) between different time points and α7HMZ and WT in RNA-seq. 10:30, ZT3.5; 13:30, ZT6.5; 20:30, ZT13.5. **(B)** Differential gene expression at 10:30 AM. Colored spots, log2FC ≥ 1.75 (blue, WT; red, α7HMZ). **(C)** Average FPKM values for the top 85 expressed TFs in WT fed livers at 10:30 AM, sorted by WT FPKM values at 13:30. Arrows, LETFs. * padj ≤ 0.01. **(D, E)** Average FPKM of indicated genes. # padj ≤ 0.05; (#) padj = 0.055 (p=0.01); * padj ≤ 0.01. See also Supplementary Figure 2.

10.3389/fendo.2023.1266527

livers at 10:30 AM (ZT3.5), including several cytochrome P450 (*Cyp*) genes and the NR gene CAR (*Nr1i3*) (Figure 2B).

To examine the impact of P2-HNF4α on other NR genes, we compared the FPKM values of all NR genes across all three time points. HNF4α was the most highly expressed NR in both WT and α7HMZ; the next most abundant NR, *Rxra*, was expressed at roughly 25% the level of *Hnf4a* (Supplementary Figure 2A). While most NRs displayed similar circadian oscillations in WT and α7HMZ livers, there were some notable exceptions: CAR (*Nr1i3*) was significantly downregulated in α7HMZ at all three time points (Supplementary Figure 2A, *arrow*). Rev-Erbβ (*Nr1d2*), RORγ (*Rorc*) and PPARα (*Ppara*), all involved in the transcriptional feedback loop that drives circadian expression in the liver (28), exhibited significantly reduced expression in α7HMZ livers at one time point (Supplementary Figures 2B), again suggesting a decreased responsiveness to the clock.

HNF4α is one of the most highly expressed TFs in the liver

Consistent with the relative abundance of HNF4α protein in the adult liver (1, 32), HNF4α had one of the highest transcript levels of any TF, higher even than subunits of RNA polymerase II (e.g., *Polr2m*, *Polr2b*) (Figure 2C). The other liver-enriched TFs (LETFs, *Cebpa*, *Onecut2*, *Foxa1*, *Hnf1a*, *HNF1b*) had transcript levels at least 10-fold lower than *Hnf4a* (Figure 2C, *inset*, *arrows*), consistent with HNF4α being a major regulator of liver-specific gene expression. Several TFs showed statistically significant differences between WT and α7HMZ (Figure 2C, *asterisk*), including those known to play a role in sexual dimorphic gene expression (*Stat5a*, *Stat5b*, *Ahr*, *Nr0b2*) (Figure 2D and Supplementary Figure 2B) (33, 34). Interestingly, *Esr1* (estrogen receptor alpha, ERα) expression was significantly upregulated in α7HMZ while *Ar* (androgen receptor, AR) was downregulated (Figure 2E), suggesting a potential "feminization" of the α7HMZ liver.

P2-HNF4α dysregulates the expression of genes involved in fatty acid, steroid and xenobiotic/drug metabolism

HNF4α is a known regulator of Phase I and Phase II enzymes involved in the detoxification of drugs and xenobiotics (35) and has been computationally linked to sexually dimorphic and circadian expression of those genes (36). Therefore, we examined the level of expression of all cytochrome P450 (*Cyp*) genes (Phase I) as well as glutathione S-transferases (*Gst*) and UDP glucuronosyltransferases (*Ugt*) (Phase II). While the diurnal pattern of expression was generally the same in WT and α7HMZ, the absolute level of expression was often altered (Figure 3A). For example, the expression of *Cyp2c50* and *Cyp2c54*, which encode enzymes that metabolize linoleic acid, the endogenous HNF4α ligand (37), was much lower in α7HMZ livers (Figures 1E, 3A). Several *Ugt* genes were dysregulated and metabolomic analysis revealed a significant (padj <0.01) decrease in UDP glucuronic acid in α7HMZ livers (Figure 3A, *bottom*). Since glucose is needed to make UDP glucuronic acid, this decrease could be linked to carbohydrate metabolism.

The NR CAR (*Nr1i3*) is downregulated 10- to 18-fold in α7HMZ mice (Figure 3B), as reported previously (23), and could explain some of the changes in *Cyp* gene expression observed in α7HMZ livers (38). In contrast, the expression of PXR (*Nr1i2*), which is known to co-regulate many Phase I and II genes with CAR and to be upregulated by HNF4α in fetal liver (38, 39), was not altered (Supplementary Figure 2C), suggesting that the primary role of P2-HNF4α in the adult liver may not be to regulate xenobiotic metabolism.

In addition to *Cyp2c50/54*, transcript levels of other fatty acid metabolic enzymes were also decreased in α7HMZ livers. *Cyp2b10* and *Ephx2* (Figure 3C), which convert arachidonic acid to oxylipins via a two-step process (40), were significantly downregulated, as were all four DiHETrE products of arachidonic acid in the CYP2B10-EPHX2 pathway (Figure 3D), confirming a phenotypic effect on fatty acid metabolism. Changes in gene expression in the steroid metabolism pathway were also observed in α7HMZ livers with an increase in *Cyp17a1* and a decrease in *Srd5a1* and *Hsd3b5* (Figure 3E). CYP17A1 plays a predominant role in steroid hormone biosynthesis, while steroid 5-alpha-reductase (*Srd5a1*) metabolizes the conversion of testosterone into the more potent dihydrotestosterone (DHT) and 3 beta-hydroxysteroid dehydrogenase type 5 (*Hsd3b5*) is typically lower in female livers (41). Tellingly, several of the most significantly increased transcripts in α7HMZ livers, including *Cyp2b9*, *Cyp2b13 and Cyp2a4* (Figure 3F), are female-specific, have testosterone hydroxylase activity and are known to be regulated by HNF4α (42). Furthermore, *Ephx2* expression and activity is downregulated by estrogen (43), which could explain the observed decrease in DiHETrEs in α7HMZ livers. All told, these results are consistent with the "feminization" of the α7HMZ livers suggested by the increase in ERα and decrease in AR expression (Figure 2E).

P1- and P2-HNF4α isoforms have similar but non-identical DNA binding profiles both *in vivo* and *in vitro*

To determine whether the P2-HNF4α transcriptional program is due to alterations in chromatin binding, ChIP-seq analysis was performed at 10:30 AM (ZT3.5) using an antibody (α445) that recognizes both isoforms (Figure 1A). Consistent with the high level of expression of the *Hnf4a* gene, there was a large number of HNF4α binding events in both WT and α7HMZ livers (~40,000 peaks). While the vast majority of peaks were similar in the two sets of mice, ~1.4 to 2.6% of the peaks were enriched for a particular isoform (WT unique: 572 peaks; α7HMZ unique: 1067 peaks) (Figure 4A). Analysis of the feature distribution of the ChIP peaks shows that both WT- and α7HMZ-unique peaks were less frequently located in the promoter region (≤ 2kb from +1) than the common peaks and the α7HMZ-unique peaks were enriched in intronic regions (Figure 4B).

Motif mining showed that the most common motif in both the WT and α7HMZ unique peaks was an HNF4α motif (xxxxCAAAGTCCA).

10.3389/fendo.2023.1266527

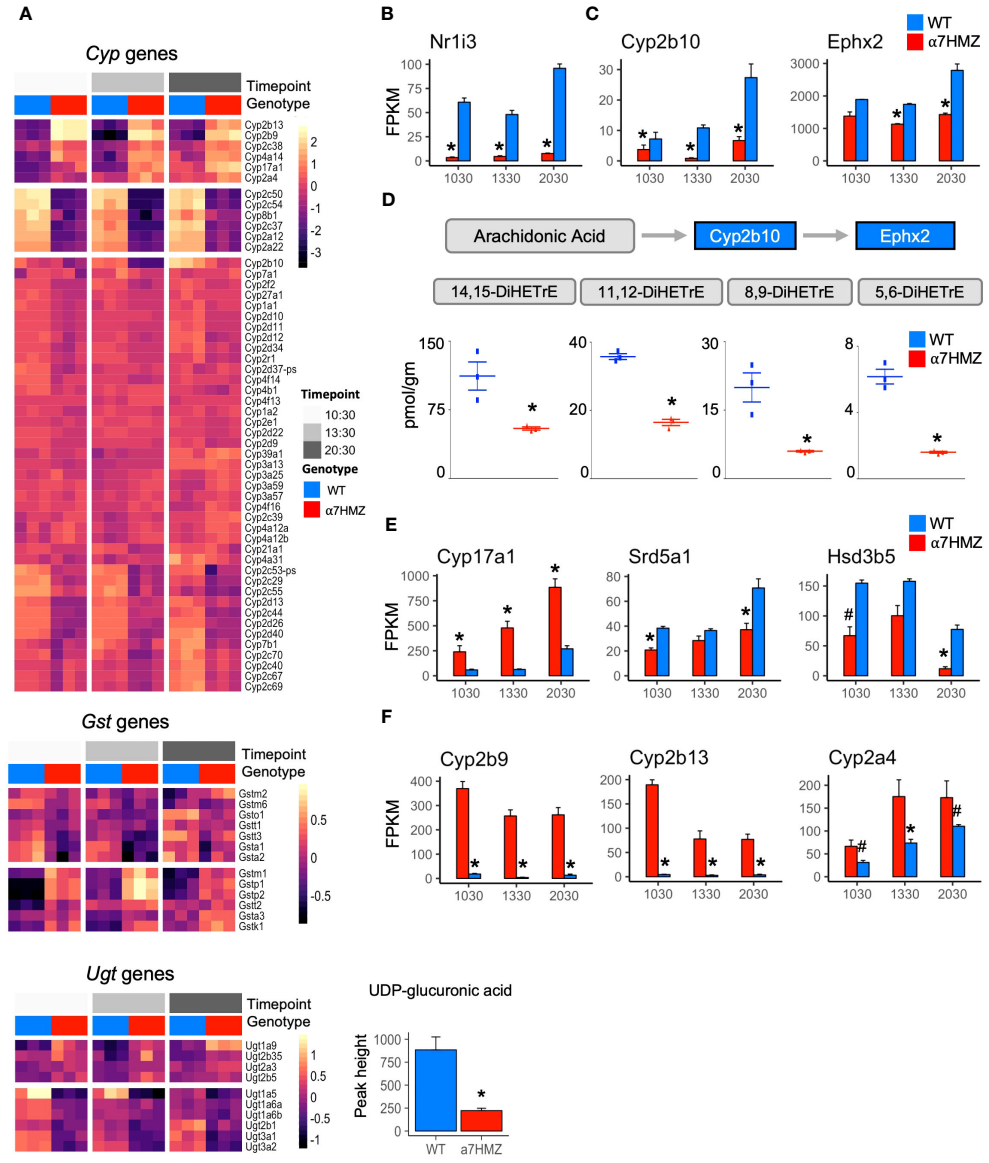

FIGURE 3
P2-HNF4α dysregulates the expression of genes involved in fatty acid, steroid and xenobiotic/drug metabolism. **(A)** Heatmap of row-normalized rlog read counts from RNA-seq for Phase I and II genes (padj ≤ 0.01) between WT and α7HMZ at any time point. *Bottom*, level of UDP-glucuronic acid in WT and α7HMZ livers, * p ≤ 0.01 by Mann-Whitney. **(B, C, E, F)** Average FPKM values. * padj ≤ 0.01 and # padj ≤ 0.05 between WT and α7HMZ at a given time point. **(D)** DiHETrE oxylipins (or DHETs, dihydroxytrienoic acid) levels in WT and α7HMZ livers (n=3, 12-13 weeks old), generated from arachidonic acid by CYP2B10 and EPHX2. * p ≤ 0.01 by Student's T-test.

To determine whether there might be additional TFs bound in those peaks, we analyzed the DNA sequence of the uniquely bound peaks with an HNF4α-trained support vector machine (SVM) algorithm and categorized the peaks into one of four categories (>2, 2 to 1.75, 1.75 to 1.5 and 1.5 to 1.25 SVM score) based on the single highest-scoring SVM motif within the peak. All but a few peaks fell into one of these categories suggesting that the isoform-specific peaks are likely due to direct binding to the DNA. Nonetheless, *de novo* motif calling with MEME-ChIP revealed different TF motifs in some of the isoform-specific peaks. CEBPA and FOX were the only motifs significantly enriched in WT-unique peaks, but several motifs were found in α7HMZ-unique peaks, including SOX, GATA5, SMAD2, ETS, CEBPB, FOX and PAR bZIP (Figure 4C).

To investigate the innate DNA binding specificity of the HNF4α isoforms, we designed PBMs with variations on HNF4α consensus motifs (a direct repeat with a spacing of 1, DR1, AGGTCAxAGGTCA, or DR2, AGGTCAxxAGGTCA), as well as genomic sequences mined from HNF4α ChIP-seq peaks (Figure 4D, *top middle*). In total, ~44,000 test sequences were spotted in quadruplicate on a glass slide and probed with human HNF4α2 or HNF4α8 ectopically expressed in COS-7 cells or with liver nuclear extracts (NEs) from WT and α7HMZ mice (HNF4α2/

10.3389/fendo.2023.1266527

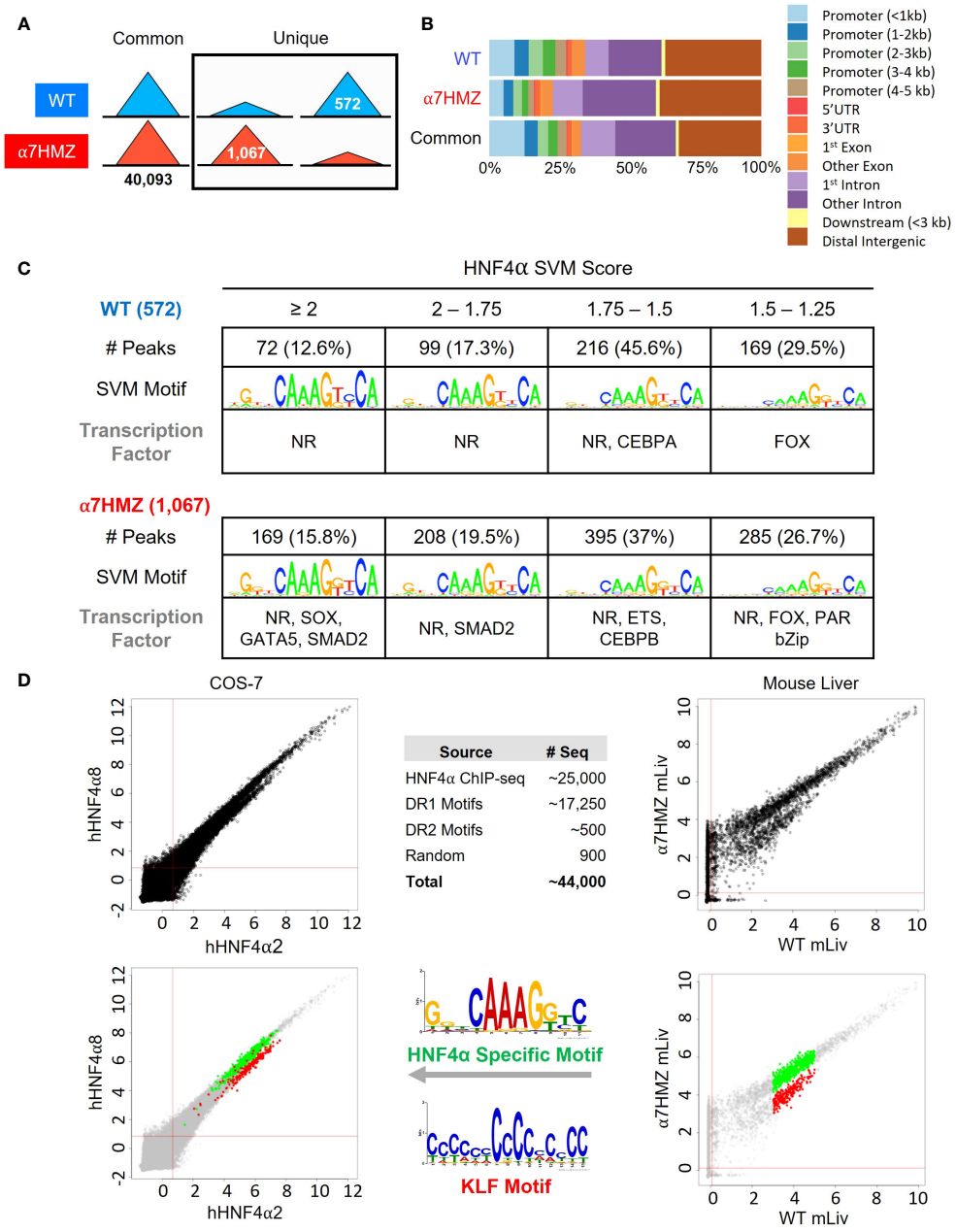

FIGURE 4
HNF4α isoforms exhibit similar but non identical chromatin binding profiles *in vivo* and *in vitro*. **(A)** Number of common, WT- and α7HMZ-unique HNF4α ChIP-seq peaks. **(B)** Feature distribution plots from ChIPseeker. **(C)** WT- and α7HMZ-unique ChIP peaks grouped by HNF4α SVM motif score. TFs corresponding to the top DNA motifs from *de novo* MEME-ChIP analysis are given. NRs, HNF4α DR1-like motif. See also Supplementary Figures 3, 4. **(D)** Log2 average binding intensities from PBMs with ectopically expressed human HNF4α8 versus HNF4α2 in COS-7 cells, and mouse liver NEs from α7HMZ versus WT; test sequences shown are from HNF4α ChIPseq peaks in Caco-2 cells. *Middle top*, test sequences used in entire PBM design. *Middle bottom*, PWMs for red (KLF Motif, boottom spur) and green (HNF4α Specific Motif, top spur) spots in mouse liver scatterplot, which are mapped back onto COS-7 plots. See Supplementary Table 5 for data plotted in these graphs.

α8 have a 10-amino acid insertion in the F domain of HNF4α1/α7, respectively). Scatter plot analysis of the PBM scores verified that the two HNF4α isoforms exhibited nearly identical DNA binding affinity and specificity across all test sequences in the COS-7 extracts; shown are the results from ~25,000 sequences derived from the ChIP-seq (Figure 4D, *top left*). Liver NEs from WT and α7HMZ mice were also nearly identical except for a subset of sequences that differed between WT and α7HMZ (Figure 4D, *top right*). Motif analysis of the two groups of sequences, shown in green (top spur, HNF4α specific motif) and red (bottom spur, KLF motif), revealed a preference for HNF4α in WT livers for GC-rich sequences recognized by SP1/KLF proteins (Figure 4D, *bottom right, middle*). A similar, albeit less pronounced, preference was noted in the COS-7 extracts (Figure 4D, *bottom left*). Consistently,

10.3389/fendo.2023.1266527

HNF4α1 has been found to interact with SP1 both on and off chromatin, an interaction that involves the N-terminal domain of HNF4α1 (44–46).

HNF4α isoforms have unique interactomes

To assess the contribution of differential chromatin binding to changes in gene expression, we cross-referenced the ChIP-seq and RNA-seq datasets at the 10:30 AM time point and found that ~22% of WT-specific (62 out of 294) and α7HMZ-specific genes (41 out of 181) have one or more unique ChIP peaks within 50 kb of the transcription start site (TSS, +1) (Figure 5A). WT-specific genes matching these criteria include *Nr1i3*, *Cyp2c50*, *Cyp2c54*, *Rarres1*, *Fmn1*, *Cdhr5*, and *Camk1d*, while α7HMZ-specific genes include *Cyp2b9*, *Fgfr1*, *Wnk4*, *Cyp4a14*, *Ppl*, *Vnn1*, *Acot1*, and *Cyp17a1* (Supplementary Table 2). Many of the most dysregulated genes contained differentially bound peaks within ~5 kb of +1 – *Nr1i3*, *Apoa4, Cyp2c50, Cyp2c54, Cyp2b9, Cyp4a14, Acot1, Cyp17a1,Ucp2, Cyp2d26* and *Treh* (Figures 5B, C and Supplementary Figure 4A, B). While the differential peaks were typically not the only nor the largest peak in the gene, they could reflect rapid cycling on and off the DNA with functional consequences.

Since the majority of dysregulated genes had no nearby HNF4α isoform-specific ChIP peak, we examined HNF4α protein-protein interactions in WT and α7HMZ livers by RIME at 10:30 (ZT3.5) and 20:30 (ZT13.5). Both time points yielded a considerable number of interacting proteins at least eight-fold above the background, including many proteins that bound a single isoform (10:30: 167 WT-specific, 108 α7HMZ-specific; 20:30: 357 WT-

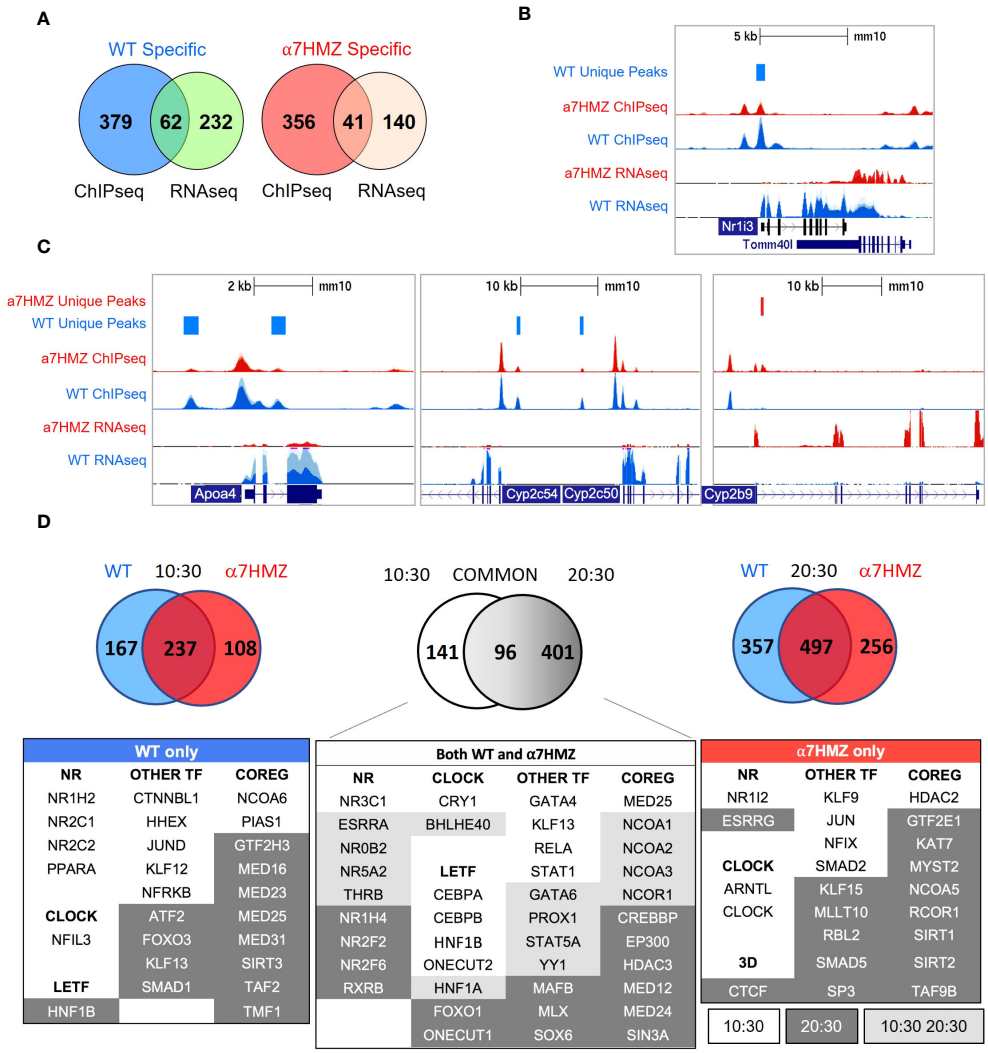

FIGURE 5
HNF4α isoforms have unique protein-protein interactions. **(A)** Number of genes with one or more WT- or α7HMZ-unique ChIP-peaks within a 50-kb of +1 of differentially expressed genes in WT and α7HMZ livers (padj ≤ 0.01). **(B, C)** UCSC Genome Browser view of dysregulated genes with a unique ChIP-signal and RNA-seq from 10:30 AM. Axes for WT and α7HMZ signals are set to the same scale but may differ between genes. **(D)** *Top*, number of proteins bound to HNF4α in WT vs. α7HMZ livers at 10:30 (ZT3.5 *left*), at 20:30 (ZT13.5 *right*) and in both WT and α7HMZ at 10:30 vs. 20:30 (*middle*). *Bottom*, select proteins involved in transcription regulation bound only in WT, α7HMZ or both genotypes. See Supplementary Figure 4D for interactions with signaling proteins and Supplementary Table 3 for all interacting proteins.

specific, 256 α7HMZ-specific) (Figure 5D, *top*). There was considerable overlap between the common groups for the two time points (96 proteins bound HNF4α in both WT and α7HMZ livers at both time points), underscoring the robustness of the method. There were also many proteins that bound both isoforms but only at a single time point (10:30: 141; 20:30: 401). Notably, core circadian regulator CRY1 bound HNF4α in both WT and α7HMZ livers but only at 10:30 AM (Figure 5D, *bottom*). In contrast, BHLHE40 bound both isoforms at both 10:30 and 20:30, while NFIL3 uniquely bound in WT livers and ARNTL (BMAL1) and CLOCK in α7HMZ but only at 10:30 (Figure 5D, *bottom*). These findings are consistent with recent reports of HNF4α interacting with the clock machinery and playing a role in maintaining circadian oscillations in the liver (29).

Several LETFs interacted with both isoforms but only at one time point (10:30 only: CEBPA, CEBPB, HNF1B, ONECUT2; 20:30 only: FOXO1, ONECUT1); only HNF1A interacted at both time points (Figure 5D, *bottom, middle*). Many NRs interacted with HNF4α in both WT and α7HMZ livers, including NR3C1(GR) and NR0B2 (SHP), both of which have been shown previously to functionally interact with HNF4α, further validating the RIME results (47, 48). There were also isoform-specific interactions, mostly with WT at 10:30 (NR1H2, NR2C1, NR2C2, PPARA). Interestingly, xenobiotic receptor PXR (NR1I2) interacted with HNF4α but only in α7HMZ livers at 10:30 (Figure 5D, *bottom left* and *right*). While the expression of *Nr1i2* was not changed in α7HMZ livers (Supplementary Figure 2C), an environmental estrogen that activates PXR has been shown to increase the expression of two female-specific Cyp genes (*Cyp2b9* and *Cyp2a4*) in male mice: both are significantly upregulated in α7HMZ livers and bound by HNF4α (Figure 5C and Supplementary Table 2) (49). HNF4α in α7HMZ livers also uniquely interacted with ESRRG (ERRγ, *Nr3b3*) but only at 20:30: ERRs play important roles in mitochondrial biogenesis and function, including fatty acid oxidation (50). Interestingly, ERR DNA binding motifs were found in α7HMZ ChIP peaks but not WT (Supplementary Figure 3B).

There were many other TFs and co-regulators that interacted with a single HNF4α isoform, often in a circadian fashion (Figure 5D, *bottom*), which could explain the observed differential gene expression between WT and α7HMZ. Several of these proteins were previously confirmed by more conventional means (31, 51–53). Finally, there were several signaling molecules that interacted uniquely with the isoforms and at distinct time points – one or more of these could also contribute to isoform-specific gene expression, independent of ChIP peaks (Supplementary Figure 4D).

HNF4α isoforms differentially impact circadian gene expression

Interactions with circadian TFs suggest that HNF4α may play a role in the hepatic clock. Analysis of all DEGs between any two time points (10:30, 13:30 or 20:30; padj<0.01 and log2FC>2) for either WT or α7HMZ yielded 53 genes, including commonly known circadian genes (*Cry1*, *Rorc*, *Dbp*, *Bhlhe41*, *Usp2*, *Per2*, *Per3*, *Arntl*, and *Nr1d1*) as well as many metabolism-related genes (*Fmo3*, *Lpl*, *Car3*, *Corin*, *Npas2*, *Hmgcs1*, *Mme*, *Slc45a3*, *Hsd3b4*, *Hsd3b5*, *Slc10a2*) (Figure 6A *top*). While most of these circadian-regulated genes showed the same general profile in WT and α7HMZ livers, there were some differences in the magnitude of the circadian effect between the genotypes. For example, *Fmo3*, a drug metabolizing gene whose expression varies greatly between individuals, had a much higher expression in α7HMZ livers at 20:30. In contrast, *Aqp8*, a water channel protein important for mitochondrial respiratory function (54), had much lower levels of expression in α7HMZ at all time points (Figure 6A, *arrows*).

While the majority of the clock machinery maintained cyclic expression in both genotypes (Figure 6A *bottom*), there were significant differences in expression between WT and α7HMZ in core clock components *Arntl*, *Clock*, *Cry1*, *Nfil3*, *Npas2* and *Per3* at one or more time points (Figure 6B), as well as *Rorc* and *Ppara* (Supplementary Figure 2B). The fact that other core components of the clock machinery did not show differences between the two genotypes (e.g., *Per1*, *Per2*, *Rora*, *Bhlhe40*) (Supplementary Figure 5A) suggests that the effect of P2-HNF4α on the clock is a specific one.

A sample distance matrix further confirmed a subtle yet real effect of P2-HNF4α on the hepatic clock. While the WT replicates at a given time point are much more similar to each other than they are to other time points, α7HMZ replicates show strong self-identity only in the 13:30 samples (Figure 6C). This is despite the fact that a principal component analysis (PCA) showed a good separation and categorization of each sample group (Supplementary Figure 7A).

P2-HNF4α is expressed at discrete times in the normal adult liver

While expression of P2-HNF4α protein in the normal adult liver has not been previously reported, this could be due to the time of day that livers are typically harvested (before midday). Since the current results show links between P2-HNF4α in α7HMZ livers and the circadian clock, we harvested livers from WT mice at four time points (ZT3, ZT9, ZT15, ZT21) and looked for P2-HNF4α mRNA by RT-qPCR and protein by immunoblot (IB). The results show expression of P2-HNF4α at ZT9 (4 PM) and ZT21 (4 AM) and a further increase in *Clock* KO livers. In contrast, P1-HNF4α RNA and protein levels did not oscillate in either WT or CLOCK KO mice (Figure 6E, Supplementary Figures 5B, C).

Metabolomic profiling indicates a role for P2-HNF4α in ketogenesis

Since metabolism is tightly linked to the clock in the liver (55–57), we performed metabolomic analysis of primary metabolites and complex lipids on WT and α7HMZ livers at 10:30 AM (ZT3.5). Nearly one-quarter of the primary metabolites (100 out of 369 total)

10.3389/fendo.2023.1266527

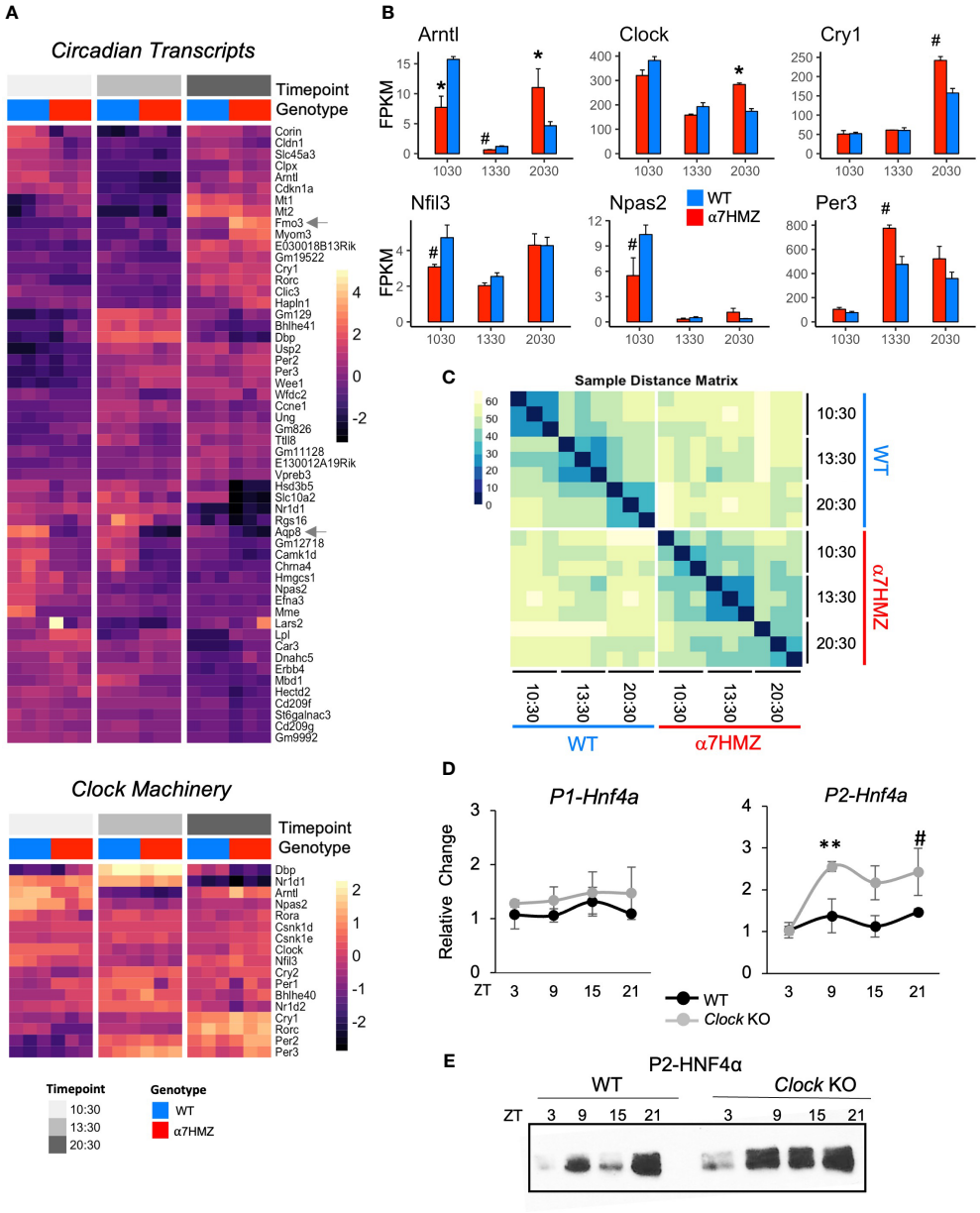

FIGURE 6
HNF4α isoforms differentially impact diurnal gene expression. **(A)** Heatmap of rlog read counts for all circadian-regulated and core clock genes with padj ≤ 0.01 and log2FC ≥ 2 between any pair of time points. 10:30, ZT3.5; 13:30, ZT6.5; 20:30 ZT13.5 **(B)** Average FPKM of select circadian clock genes. # padj ≤ 0.05; * padj ≤ 0.01. **(C)** Sample distance matrix for each RNA-seq replicate, calculated across the full transcriptome. The darker the color, the higher the degree of similarity. **(D)** Relative fold increase in P1- and P2-HNF4α in livers of WT or littermate *Clock* KO by qRT-PCR at indicated ZT. Two-way ANOVA, Sidak's multiple comparisons test, # p ≤ 0.05; ** p ≤ 0.005. Error bars, SEM (n=3-4). **(E)** Representative IB of diurnal expression of P2-HNF4α protein in WCE from WT and *Clock* KO livers using P2-specific antibodies (n=3-4). See also Supplementary Figure 5.

were significantly down-regulated (p <0.05) in α7HMZ livers (Figure 7A, up in WT). Metabolite Set Enrichment Analysis showed that the top four enriched categories in WT are involved in carbohydrate metabolism and protein biosynthesis (Supplementary Figure 6A). Glucose and pyruvate were both significantly down in α7HMZ livers (Figure 7B), as was PEPCK (*Pck1*), an important enzyme in gluconeogenesis (Supplementary Figure 6B). Genes in pathways downstream of pyruvate were also significantly decreased in α7HMZ, including lactate dehydrogenase (*Ldha*, *Ldhd*), pyruvate carboxylase (*Pcx*) and citrate synthase (*Cs*) in the Kreb's cycle (Supplementary Figure 6C), as was citric acid, a key intermediate in the cycle (Figure 7B). Kreb's intermediates oxalic and succinic acid were also reduced although they did not reach significance (Supplementary Figure 6D). In contrast, genes involved in the formation of ketone bodies were upregulated in α7HMZ (*Hmgcs2*, *Hmgcl*) (Supplementary Figure 6E), as was the ketone body β-hydroxybutyric acid (Figure 7B), as previously reported (23). Levels of hundreds of complex lipids were altered

10.3389/fendo.2023.1266527

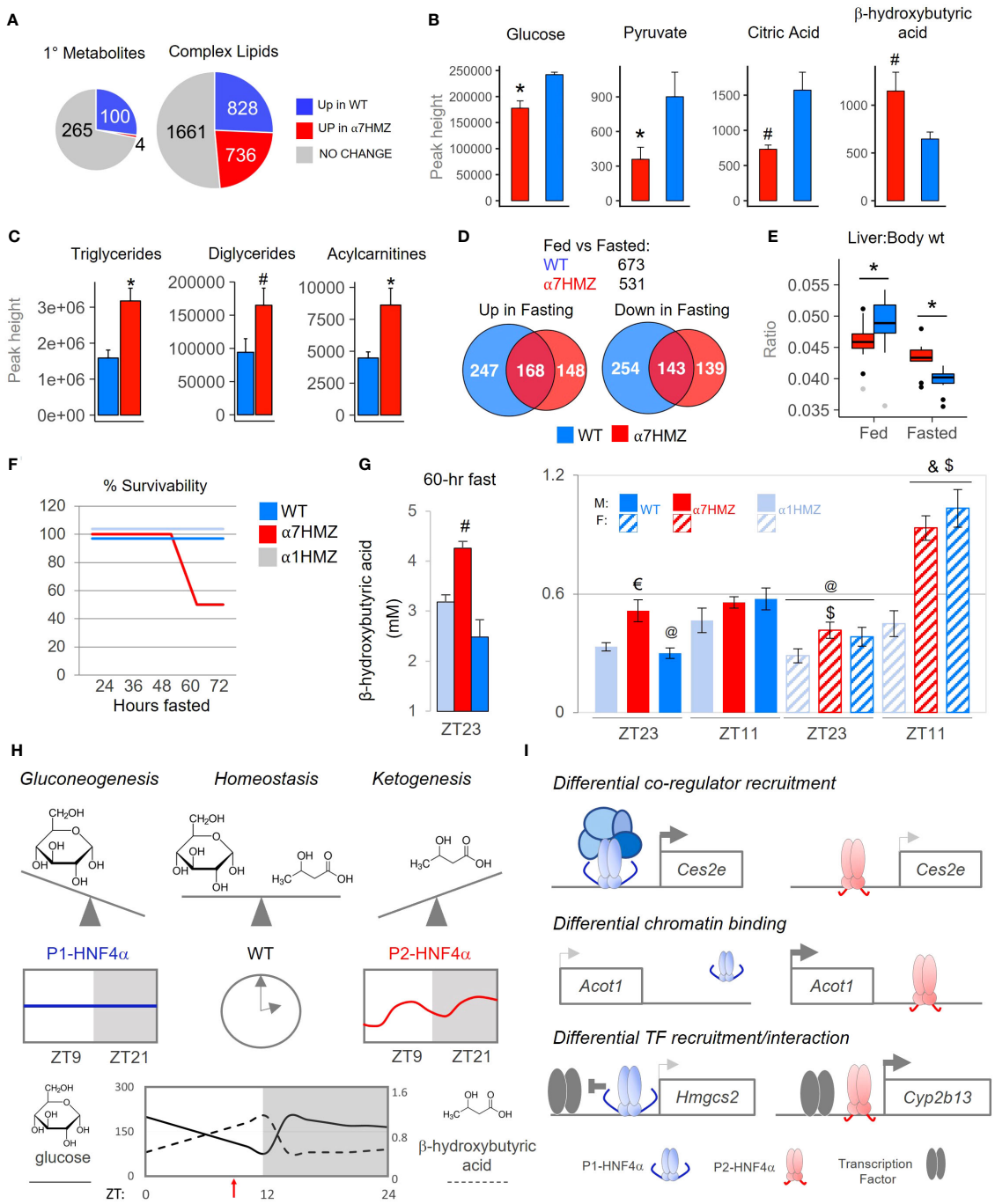

FIGURE 7
P1-HNF4α drives gluconeogenesis while P2-HNF4α drives ketogenesis; both are required for homeostasis in carbohydrate and lipid metabolism. **(A)** Number of primary metabolites and complex lipids in WT and α7HMZ livers of fed mice at 10:30 AM (n=8 per group). Uniqueness identified by Mann-Whitney U-test ($p \leq 0.05$). **(B, C)** Primary metabolites related to Krebs cycle and ketogenesis [a single mouse outlier was omitted for both the WT and α7HMZ datasets for a final n=7 per group, **(B)**] and known complex lipids [n=8 per group, **(C)**]. Student's T-test: # $p \leq 0.05$; * $p \leq 0.01$. **(D)** Number of genes dysregulated (padj ≤ 0.01) in fed vs. fasted (12 hr) WT and α7HMZ livers (10:30 AM). **(E)** Liver-to-body weight ratios in fed and fasted WT and α7HMZ mice (n = 9-14). * $p \leq 0.01$ by Student's T-test, excluding outliers (gray dots). **(F)** Percent survival of WT, α1HMZ and α7HMZ male mice (~20 wks) during a prolonged fast (n=5-6). **(G)** β-hydroxybutyric acid levels in blood of WT, α7HMZ and α1HMZ during a 60-hr fast (*left*) (n=3-5) and at ZT23 and ZT11 after 1 week of restricted feeding (food removed between ZT0 and ZT12) (*right*) (n = 6-8). Student's T-test: # $p<0.05$ vs. other two genotypes; $ $p<0.05$ vs. α1HMZ females at the same time point; & $p<0.05$ vs. males of same genotype at ZT11; @ $p<0.05$ vs. females of the same genotype at ZT11; € $p<0.05$ vs. WT and α1HMZ males at ZT23. **(H, I)** Models discussed in text; see also Supplementary Figures 6, 7. See Supplementary Table 4 for complete metabolomics data.

10.3389/fendo.2023.1266527

(up or down) in α7HMZ livers, including a notable increase in total triglycerides, diacylglycerides and acylcarnitines in the α7HMZ liver and a decrease in phospholipid species (Figures 7A, C and Supplementary Figure 6F).

Since ketone bodies are elevated upon fasting, we performed RNA-seq on livers from 12-hr fasted WT and α7HMZ mice. The transcriptomes for both WT and α7HMZ fasted livers were quite distinct from the fed time points as well as from each other (Supplementary Figures 7A, B): WT mice had more genes altered upon fasting (673 versus 531 in α7HMZ) as well as more WT-specific genes either up- or downregulated (Figure 7D). Liver-to-body weight ratios were significantly lower in α7HMZ versus WT fed mice; in contrast, in fasted livers the ratio was lower in WT (Figure 7E). Since WT mammals are known to store fat in their liver during periods of fasting and since fasted α7HMZ livers accumulate more fat than WT mice (Figure 7C) (23), these results suggest that P2-HNF4α might promote a "fasting-response" program, consistent with the expression of P2-HNF4α at ZT9, near the end of the daily fasting period.

However, when the mice were subjected to a prolonged fast, unexpectedly, 50% of the α7HMZ mice died after ~60 hrs; in contrast, α1HMZ and WT mice survived a full 72 hrs without food (Figure 7F). Mortality was not due to hypoglycemia as blood glucose levels did not drop below 65 mg/dL; in fact, they increased after 48 hrs of fasting at ZT11, especially in α1HMZ (Supplementary Figure 7C). In contrast, circulating ketone bodies were highly elevated in the α7HMZ mice that survived the 60-hr fast (4.25 mM) (Figure 7G), and suggested that the α7HMZ mice undergoing a prolonged fast might have died of ketoacidosis.

Since the α7HMZ transcriptome showed signs of "feminization" and since females tend to have higher levels of ketone bodies than males (24, 58), we examined whether the elevated levels of ketone bodies in WT females is due to the ability to express P2-HNF4α. As anticipated, in WT mice ketone bodies were higher near the end of the daily fast (ZT11, 7 PM) than at the end of the feeding period (ZT23, 7 AM), in both males and females (Figure 7G). In contrast, α7HMZ males had ketone bodies at ZT23 nearly as high as at ZT11. Importantly, α7HMZ and WT females had much higher levels of ketone bodies at ZT11 than their male counterparts, whereas the α1HMZ females had levels similar to α1HMZ males and much lower than either WT or α7HMZ females (Figures 7G). This suggests that P2-HNF4α is required for the elevated levels of ketone bodies in females.

Discussion

While many mammalian genes have multiple promoters that drive expression of proteins with alternative N-termini, the physiological relevance of those different isoforms is seldom known. Using exon-swap mice and omics approaches, we show for the first time that the alternative isoform of the *Hnf4a* gene (P2-HNF4α), previously thought to be expressed only in fetal liver and liver cancer, plays an important metabolic role in the adult liver and is implicated in both the circadian clock and sex-specific gene expression.

Both P1- and P2-HNF4α are required for metabolic homeostasis in males and females

The "P2-HNF4α program" is characterized by a decrease in carbohydrate metabolism and an increase in hepatic fat storage, as well as ketogenesis, which typically occur during periods of fasting (59). Altered expression of genes involved in fatty acid oxidation or oxidative phosphorylation in the mitochondria are consistent with a shift from carbohydrates to fatty acids as an energy source (e.g., *Hmgcs2*, *Acot1*, *Ucp2*, Figure 1F and Supplementary Table 2). In contrast, it appears that P1-HNF4α drives gluconeogenesis and is required to temper the P2-HNF4α response to avoid ketoacidosis under conditions of stress, such as fasting. Only WT mice, which express both HNF4α isoforms in the liver, achieve homeostatic balance between carbohydrate and lipid metabolism (Figure 7H). We propose that this balance is achieved on a daily basis by upregulating P2-HNF4α at the end of the fasting period (~ZT9) (Figure 7), resulting in the well characterized elevation of ketone bodies right before feeding (60). Intriguingly, P2-HNF4α is also required for the elevated levels of ketone bodies in female mice (Figure 7G), consistent with a "feminization" of the α7HMZ livers and previous results showing that KO of HNF4α in the adult liver leads to a loss of male-specific genes and an increase of female-specific genes (61). Finally, P2- but not P1-HNF4α interacts with the NAD-dependent deacetylase SIRT1, which is activated upon fasting and is associated with fatty acid oxidation, ketogenesis and fatty liver (Figure 5D) (62).

Multiple mechanisms are responsible for HNF4α isoform-specific gene regulation

Our results indicate that P2-HNF4α drives its unique transcriptional program via multiple mechanisms. Differential recruitment of co-regulators to target gene promoters (Figure 5D) could explain altered expression of genes such as *Ces2e*, which encodes carboxylesterase 2, an enzyme that hydrolyzes triacylglycerols (Figure 7I *top*). Both P1- and P2-HNF4α bind the *Ces2e* promoter in a similar fashion but *Ces2e* is expressed at much lower levels in α7HMZ livers compared to WT, which could explain the elevated levels of triglycerides in α7HMZ livers (Figures 1E, 7C, Supplementary 4C). A second potential mechanism is differential binding to regulatory regions. An enriched ChIP-seq peak in α7HMZ livers, for example, could explain the upregulation of a key enzyme in β-oxidation of fatty acids, *Acot1* (Figures 7I *middle* and Supplementary Figure 4A). Similarly, a reduction in ChIP peaks could explain the decrease in expression of *Apoa4* and *Nr1i3* (CAR) in α7HMZ livers (Figures 5B, C). A third mechanism involves differential recruitment and/or interaction of TFs with a given HNF4α isoform (Figure 7I *bottom*). For example, PPARα is known to be a major player in ketogenesis, activating the expression of the mitochondrial enzyme HMGCS2 which catalyzes the first step in ketogenesis (59). P1-HNF4α has been shown to decrease *Hmgcs2* expression by repressing PPARα-dependent activation (63). This repression could be facilitated by

a unique protein-protein interaction between P1-HNF4α and PPARα (Figure 5D). In contrast, in α7HMZ livers *Hmgcs2* expression is elevated and HNF4α ChIP-seq peaks in α7HMZ livers are similar to those in WT (Supplementary Figures 4C, 6E). Similarly, specific interactions between P2-HNF4α and TFs involved in sex-specific gene expression (e.g., NR1I2, SP1 family/KLF) could contribute to increased expression of female-specific genes such as *Cyp2b13* (Figures 3F, 5D, Supplementary Figure 4C) (49). Additional mechanisms driving the P2-HNF4α program include differential interaction with signaling molecules, altered expression of other TFs, such as those that play a role in sex-specific gene expression *(Stat5b, Stat5a*, estrogen and androgen receptors) (33, 36), and elevated levels of ketone bodies which can impact histone deacetylase activity, as well as the circadian clock (64) (Figures 2, 7G, Supplementary Figure 4D).

Physiological and pathological triggers of the P2-HNF4α program

There are now three known physiological conditions in which P2-HNF4α is expressed in the liver – fetal liver and ZT9 and ZT21 in adult liver (Figure 6). Increased expression of P2-HNF4α expression right before birth (E17.5), followed by a sharp decline after birth (5, 6), could explain why the α7HMZ transcriptome is not more similar to that of the E14.5 fetal liver: rather than promoting early liver development, the role of P2-HNF4α appears to be a metabolic one, perhaps preparing the fetus to survive the birthing process and immediate postnatal period by increasing fat in the liver. The subsequent decrease in P2-HNF4α expression after birth could be mediated by GR which is induced by stress hormones released during parturition (65): GR preferentially increases the expression of P1-HNF4α (7, 66) which would in turn repress the P2 promoter (6).

Factors responsible for increased expression of P2-HNF4α at ZT9 have not been identified, but its expression seems to be required for the increased expression of ketogenic genes and ketone bodies in response to the daily fast (Figures 7B, G, Supplementary Figure 6E). The role of P2-HNF4α at ZT21 is more difficult to explain as ketone bodies are low at that time (Figure 7G) (60). Total protein synthesis is increased at ~ZT22 (67), as well as both P2- and P1-HNF4α-specific targets (Supplementary Figure 7D), so expression of P2- (and P1-)HNF4α at ZT21 could be the result of a global effect on protein synthesis.

In addition to physiological triggers, there are now four pathological conditions in which P2-HNF4α is known to be elevated in the adult liver – cancer (11, 12, 68), high fat diet (12, 20), disrupted clock (Figures 6D, E) and alcoholic hepatitis (68). In terms of cancer, our results indicate that P2-HNF4α is not oncogenic per se – the P2-HNF4α transcriptome shows only a partial overlap with HCC, key proliferation markers (Ki67 and PCNA) are not upregulated in α7HMZ livers and there is no evidence of hepatomegaly (Figures 1H, 7E, Supplementary Figures 1D,E). Furthermore, no increase in spontaneous, macroscopic tumors has been observed in α7HMZ livers, even in older mice (unpublished observation). While HCC patients with increased P2-HNF4α have a poor prognosis (13), rather than acting as an oncogene *per se*, P2-HNF4α may be upregulated simply due to a decrease in the expression of the tumor suppressor P1-HNF4α (7, 66) and inadvertently promote liver cancer progression via metabolic effects. For example, acylcarnitines are elevated in α7HMZ livers (Figure 7C, Supplementary Figure 6F) and have been identified as potential diagnostic and prognostic biomarkers for HCC (69, 70). Given the renewed interest in cancer metabolism, including in HCC, it will be of interest to determine exactly how a metabolism altered by unopposed P2-HNF4α might contribute to cancer progression and/or treatment (71). This is particularly true considering that elevated ketone bodies may trigger a protective mechanism against oxidative stress (72), which would suggest that elevated levels of P2-HNF4α in HCC may actually play a protective role. Finally, several matrix metalloproteinases (*Mmp14*, *Mmp15*, *Mmp19*), which are linked to poor prognosis of liver or colorectal cancer patients (73–75), are also upregulated by P2-HNF4α (Supplementary Table 1) and dysregulation of genes involved in drug metabolism could impact treatment of liver cancer (Figure 3).

The second condition that leads to expression of P2-HNF4α in the adult liver – high fat diet (HFD) – could be related to both cancer and the third condition, disrupted clock. We recently reported that P2-HNF4α expression is increased in the livers of mice fed a HFD and that the circadian regulator BMAL1 represses P2-HNF4α expression in HCC (12). Consistently, P2- but not P1-HNF4α interacts with BMAL1 (ARNTL) and CLOCK and the *Clock* KO increases P2- but not P1-HNF4α expression (Figures 6D, 7D, E). Dysregulation of the clock, such as during jet lag, could potentially contribute to liver cancer by upregulating P2-HNF4α (Figures 6D, E) (21). While HNF4α, including exon 1A and exon 1D, is highly conserved between mouse and human (96% identity on the protein level in BLAST) (2), given the genetic variation in regulatory regions between species, it will be of interest to determine whether P2-HNF4α expression impacts the expression of genes involved in the human hepatic metabolome (and hepatic circadian clock) in the same fashion as the mouse (76).

The fourth pathological condition where P2-HNF4α is expressed in the liver – human alcoholic steatohepatitis (68) – is consistent with increased fat in α7HMZ livers and an enrichment of genes associated with alcoholism in α7HMZ mice (Figures 1F, 7C). The TGFβ pathway is implicated in P2-HNF4α expression under this scenario; SMAD binding motifs were found in α7HMZ ChIP-seq peaks but not WT peaks (Supplementary Figure 3B).

In summary, the results presented here strongly suggest that the function of P2-HNF4α is to modulate the hepatic metabolic response in general, rather than to solely promote proliferation during fetal development and liver cancer. While the elevated levels of circulating ketone bodies in α7HMZ mice suggest that P2-HNF4α may be a player in the fasting response, other results suggest that the role of the alternative isoform of HNF4α may be more complex. For example, expression of CAR (*Nr1i3*) is significantly decreased in α7HMZ livers and yet CAR is known to be increased during fasting, due to the action of PPARα and PGC1α, along with HNF4α, on the *Nr1i3* promoter (77). Additionally, while expression of PEPCK (*Pck1*), a major driver of gluconeogenesis, did not increase after a 12-hour fast in α7HMZ livers as it does in WT animals, others have shown that P2-HNF4α can

activate the *Pck1* promoter more effectively than P1-HNF4α, at least in the presence of PGC1α (20). Taken together, the findings presented here indicate that P2-HNF4α plays an important physiological role in the normal adult liver and intersects with the circadian clock in a complex fashion that merits further investigation.

Materials and methods

(See Supplemental Methods for additional methods and details).

Animal models

Young adult (16 to 20 weeks) male WT and α7HMZ mice in a mixed 129/Sv plus C57BL/6 background (23) were fed a standard lab chow (LabDiet, #5001:13.6% fat from pork lard; 28.9% protein; 57.5% carbohydrates) and used for RNA-seq, CHIP-seq, RIME analysis (all samples from the same set of mice), and oxylipin analysis. The α7HMZ male mice used for primary metabolite and complex lipid metabolomic analysis were backcrossed to C57BL/6N for 10+ generations and used with C57BL/6N WT controls (n=8, 35 weeks of age). α7HMZ and α1HMZ (backcrossed 10+ generations into C57BL/6N) were compared to scientific C57BL/6N (WT) controls for newborn liver analysis (mixed-sex) and glucose/ketone body analysis (males and females; ~16 to 20 weeks of age). *Clock*-deficient (*Clock* KO) male mice were provided by Dr. David Weaver (78) and fed a standard rodent diet (PicoLab Rodent Diet #5053: 13.1% fat from soybean oil; 24.5% protein; 62.4% carbohydrates). All mice were fed *ad libitum* and kept in 12-hr light/dark conditions in a specific pathogen-free (SPF) facility, unless indicated otherwise, and euthanized by CO_2 asphyxiation followed by tissue harvest at the indicated time points. Care and treatment of the animals were in strict accordance with guidelines from the Institutional Animal Care and Use Committee at the University of California, Riverside (UCR), or the McGovern Medical School, UT Health.

Expression profiling (RNA-seq) and analysis

Next generation sequencing of RNA (RNA-seq) was carried out as previously described (79). WT and α7HMZ male mice were sacrificed (n=3, aged 16-18 weeks) at the indicated time points – 10:30, 13:30, 20:30 (ZT3.5, ZT6.5, and ZT13.5, respectively) – within a 30-min interval. Fasted mice had food removed from 22:30 (ZT15:30) to 10:30 AM (ZT3.5) the following day (12 hr). Libraries were submitted for 75-bp single-end sequencing with Illumina NextSeq 500 at the UCR Institute of Integrated Genome Biology (IIGB) Genomics Core. A total of 24 libraries (3 fed time points, 1 fasted time point, 2 genotypes each, 3 replicates) were multiplexed and sequenced in two separate runs, each of which yielded ~600 M reads, averaging ~50 M reads per sample.

Reads were aligned to the mouse reference genome (mm10) with TopHat v2.1.1 using default parameters except for allowing only 1 unique alignment for a given read. Raw read counts were calculated at the gene level for each sample using HTSeq v0.6.1. Library normalization was performed with EDASeq (80); within-lane normalization on GC content was performed with the LOESS method and between-lane normalization was performed with non-linear full quantile method. Normalization factors from EDASeq were used for differential expression analysis with DESeq2. Normalized read counts, FPKM (fragments per kilobase per million), and rlog (regularized log transformation) results were generated for downstream analysis.

Chromatin immunoprecipitation sequencing (ChIP-seq) and SVM analysis

ChIP-seq of isolated liver cells from WT and α7HMZ males (n=3, aged 16-18 weeks) was performed as previously described (79) using 4.2 µg of affinity-purified anti-HNF4α (α445) (1) or rabbit IgG control (Santa Cruz, cat#sc-2027). Libraries were submitted for 50-bp single end sequencing by Illumina HiSEQ 2500 at the UCR IIGB Genomics Core. Reads were aligned to the mouse reference genome (mm10) with Bowtie2. Peaks were called with MACS2 for individual samples, as well as a pooled peak dataset using the SPMR (signal per million reads) parameter. Aligned reads and MACS2 peak-sets were analyzed with DiffBind (81) with DESeq2 and library size equal to total aligned reads to identify common and uniquely bound regions of the genome. Default parameters were used unless noted otherwise. ChIP-seq peaks were called with MACS2 and then filtered on -log10(p-value) ≥ 10, to approach six-fold enrichment above control. Differentially bound peaks were identified using DiffBind with MACS2 output. Curated peak lists were generated by filtering all results on peaks with "concentration" ≥ 5; defined by DiffBind as the "mean (log) reads across all samples" in contrast. The kernel-based SVM was trained as previously described using results from independent HNF4α PBM experiments (82).

Protein binding microarrays (PBM)

Protein binding microarrays (PBMs) were carried out as previously described (82). Nuclear extracts (NE) were prepared from COS-7 cells transiently transfected via $CaPO_4$ with HNF4α expression vectors for human HNF4α2 (NM_00457) and HNF4α8 (NM_175914) essentially as previously described (83). Liver NE from WT and α7HMZ mice were prepared as previously described (37). A custom-designed array was ordered from Agilent (SurePrint G3 Custom GE 4x180k), which contained oligonucleotides ~60 nucleotides (nt) in length comprised of: sequences within 100 bp of the center of HNF4α ChIP-seq peaks from human colon cancer cells (proliferative Caco-2) (84) were taken in 30-nt windows moving 5 nt at each step (~25,000 sequences); 17,250 permutations of canonical HNF4α DR1 motifs (5'- AGGTCAAA GGTCA -3'); 500 permutations of DR2 motifs with variable spacer (5'- AGGTCNNNNGGTCA -3'); ~900 random control 13-mer DNA sequences and ~170 positive controls. A total of ~44,000 test sequences were spotted in quadruplicate on the slide as single-stranded DNA for a total of ~176,000 spots of DNA. The DNA was made double-stranded

and transiently transfected Cos-7 cells expressing human HNF4α2 or human HNF4α8 or liver NEs from adult male mice fed a standard rodent diet were applied. HNF4α binding was imaged with 2-μm resolution using Agilent G2565CA Microarray Scanner at the UCLA DNA Microarray Core. Extraction and normalization of the data were as described previously (82) using gProcessedSignal from Agilent software with background correction. PWMs were generated using seqLogo. See Supplementary Table 5 for PBM results from the Caco-2 ChIPseq peaks (~25,000 unique sequences) presented in Figure 5C and the PBM Project at Synapse.org for the entire dataset.

Rapid immunoprecipitation and mass spectrometry of endogenous proteins (RIME)

RIME was performed as previously described (85) with slight modifications. Livers from the same mice used for the RNA-seq and CHIP-seq – WT and α7HMZ males n=3, 16-18 weeks of age sacrificed at 10:30 (ZT 3.5) or 20:30 (ZT13.5) – were crosslinked and IP'd with the P1/P2 antibody. Multidimensional protein identification technology (MudPIT) analysis was performed by the UCR IIGB Proteomics Core. Raw MS1 and MS2 spectra were processed with Proteome Discoverer 2.1 (Thermo Scientific) and submitted to Mascot search engine to match against NCBI non-redundant mouse protein database. Only proteins with 1% FDR cut-off ($q \leq 0.01$) were considered for subsequent analysis. Area under the curve, as reported by Proteome Discoverer, was averaged together for WT and α7HMZ samples (n=3) at each time point. IgG samples (n=3) from both WT and α7HMZ were averaged together to create a background sample. Areas were converted to log2 scale and the fold-change above IgG background was calculated for the WT and α7HMZ samples. Proteins with less than 8-fold change above background were omitted. Similarly, a 8-fold difference between WT and α7HMZ samples was used to identify unique protein interactions.

Primary metabolite, complex lipids and oxylipin analysis

All metabolomic analysis was performed at the West Coast Metabolomics Center at the University of California Davis as described previously (86) using liver tissue rinsed in cold PBS, snap frozen and stored in liquid nitrogen. Data (pmol/gm tissue or peak height) are presented as mean +/- standard error of mean (SEM). Student's T-test was used to determine statistical significance ($p < 0.05$) using GraphPad Prism v6.

Primary metabolite (carbohydrates and sugar phosphates, amino acids, hydroxyl acids, free fatty acids, purines, pyrimidines, etc.) and complex lipid analysis (87) was on WT (C57BL/6N) and α7HMZ (backcrossed into C67BL/6N) male mice harvested mid-morning and fed the standard chow (n=8, aged 38 weeks). Fold-enrichment was performed using MetaboAnalyst (88). One outlier from each group was removed before plotting and statistical analysis. Analysis of non-esterified oxylipins was performed on a mixed 129/Sv plus C57BL/6 background WT and α7HMZ males (n=3 per group, aged 12-13 weeks). Tissue homogenates (100 mg) were extracted by solid phase extraction and analyzed by ultrahigh performance liquid chromatography tandem mass spectrometry (UPLC-MS/MS) (Agilent 1200SL-AB Sciex 4000 QTrap) as previously described (89, 90). Analyst software v.1.4.2 was used to quantify peaks according to corresponding standard curves with their corresponding internal standards.

Quantification and statistical analysis

Differential gene expression (DEG) was measured using raw read counts with DESeq2: statistical significance was defined as adjusted p-value (padj) ≤ 0.01, unless otherwise noted. Legends denote thresholds using log2 fold change (log2FC) cutoffs. R library "gage" was utilized to identify differentially enriched KEGG pathways in Figure 1. Heatmaps were generated with pheatmap package in R; data were row-normalized before plotting, except for NR heatmap in Supplementary Figure 2. Transcription Factor (TF) rankings for Cleveland plots were ordered at the 13:30 (peak HNF4α expression) then manually curated with the aid of PANTHER (Mi et al., 2017). Venn diagrams were generated by the VennDiagram package in R. Unique and common RIME results were submitted to DAVID for ontology analysis. Statistical significance for primary metabolite and complex lipid data defined as $p \leq 0.05$ by Mann-Whitney U-test or Benjamini-Hochberg padj <0.05, as indicated. All barplots represent mean ± SEM; significant differences are noted between genotypes at a given time point, unless indicated otherwise. For FPKM plots, padj values are from DESeq2; in other plots, p-values are from two-way Student's T-test or One/Two-way ANOVA, as indicated. Student's Ttest was used while comparing two groups/conditions. One-way ANOVA was used for analyzing data for more than two groups that were compared for only one factor and two-way ANOVA was used for analyzing data from more than two groups that were compared for two factors. Posthoc analysis was applied for the ANOVAs to account for multiple comparisons. Standard statistical tests/programs were used for analyzing the metabolomics and transcriptomics data. External expression datasets and analysis are described in Supplemental Methods.

Data availability statement

The raw and processed RNA-seq data have been deposited in GEO under GSE117972 (https://www.ncbi.nlm.nih.gov/geo/query/acc.cgi?acc=GSE117972).

The raw and processed ChIP-seq data have been deposited in GEO under GSE231538 (https://www.ncbi.nlm.nih.gov/geo/query/acc.cgi?acc=GSE231538).

The processed PBM data (HNF4a8 PBM) have been deposited in Synapse.org under the PBM Project (DOI: https://doi.org/10.7303/syn52624564).

The raw metabolomics data (primary metabolites and complex lipids) have been deposited in Metabolomics Workbench (www.metabolomicsworkbench.org) under Project #PR000461.

Ethics statement

The animal studies were approved by Institutional Animal Care and Use Committee at the University of California, Riverside (UCR) and the McGovern Medical School, UT Health. The studies were conducted in accordance with the local legislation and institutional requirements.

Author contributions

FS: Conceptualization, Data curation, Funding acquisition, Investigation, Project administration, Supervision, Visualization, Writing – review & editing. JD: Data curation, Formal Analysis, Investigation, Methodology, Software, Visualization, Writing – original draft, Writing – review & editing. PD: Data curation, Formal Analysis, Investigation, Methodology, Visualization, Writing – review & editing. NT: Investigation, Methodology, Writing – review & editing. SR: Investigation, Methodology, Visualization, Writing – review & editing. LV: Investigation, Methodology, Writing – review & editing. JE: Investigation, Writing – review & editing. SP: Investigation, Writing – review & editing. JF: Data curation, Formal Analysis, Investigation, Methodology, Writing – review & editing. JY: Investigation, Methodology, Writing – review & editing. BH: Funding acquisition, Writing – review & editing. OF: Funding acquisition, Supervision, Writing – review & editing. BF: Investigation, Validation, Visualization, Writing – review & editing. KE-M: Funding acquisition, Supervision, Validation, Visualization, Writing – review & editing.

Funding

The author(s) declare financial support was received for the research, authorship, and/or publication of this article. The work was supported by NIH R01DK094707, DK053895 and DK127082 and USDA National Institute of Food and Agriculture (Hatch project CA-R-NEU-5680) to FS; NIEHS T32 Training Grant (5T32ES018827) and Crohn's and Colitis Foundation of America Career Development Award (#454808) to PD; WCMC Pilot Project from NIH U24 DK097154 to FS, in collaboration with OF; R01ES002710 and Superfund Research Program P42 EX004699 to BH; Start-up funds from UT Health to KE-M; NIH S10 OD010669 for the Orbitrap Fusion mass spectrometer.

Acknowledgments

We thank D Weaver for *Clock* KO mice, MC Weiss and N Briancon for HNF4α exon swap mice, J Vizcaya for assistance with newborn livers and J Martinez for uploading the ChIPseq data to GEO.

Conflict of interest

The authors declare that the research was conducted in the absence of any commercial or financial relationships that could be construed as a potential conflict of interest.

The author(s) declared that they were an editorial board member of Frontiers, at the time of submission. This had no impact on the peer review process and the final decision.

Publisher's note

Supplementary material

The Supplementary Material for this article can be found online at: https://www.frontiersin.org/articles/10.3389/fendo.2023.1266527/full#supplementary-material

References

1. Sladek FM, Zhong WM, Lai E, Darnell JE Jr. Liver-enriched transcription factor HNF-4 is a novel member of the steroid hormone receptor superfamily. *Genes Dev* (1990) 4:2353–65. doi: 10.1101/gad.4.12b.2353

2. Radi SH, Vemuri K, Martinez-Lomeli J, Sladek FM. HNF4α isoforms: the fraternal twin master regulators of liver function. *Front Endocrinol* (2023) 14:1226173. doi: 10.3389/fendo.2023.1226173

3. Battle MA, Konopka G, Parviz F, Gaggl AL, Yang C, Sladek FM, et al. Hepatocyte nuclear factor 4alpha orchestrates expression of cell adhesion proteins during the epithelial transformation of the developing liver. *Proc Natl Acad Sci USA* (2006) 103:8419–24. doi: 10.1073/pnas.0600246103

4. Hayhurst GP, Lee YH, Lambert G, Ward JM, Gonzalez FJ. Hepatocyte nuclear factor 4alpha (nuclear receptor 2A1) is essential for maintenance of hepatic gene expression and lipid homeostasis. *Mol Cell Biol* (2001) 21:1393–403. doi: 10.1128/MCB.21.4.1393-1403.2001

5. Torres-Padilla ME, Fougere-Deschatrette C, Weiss MC. Expression of HNF4a isoforms in mouse liver development is regulated by sequential promoter usage and constitutive 3 end splicing. *Mech Dev* (2001) 109:183–93. doi: 10.1016/S0925-4773(01)00521-4

6. Briançon N, Bailly A, Clotman F, Jacquemin P, Lemaigre FP, Weiss MC. Expression of the alpha7 isoform of hepatocyte nuclear factor (HNF) 4 is activated by HNF6/OC-2 and HNF1 and repressed by HNF4alpha1 in the liver. *J Biol Chem* (2004) 279:33398–408. doi: 10.1074/jbc.M405312200

7. Nakhei H, Lingott A, Lemm I, Ryffel GU. An alternative splice variant of the tissue specific transcription factor HNF4alpha predominates in undifferentiated murine cell types. *Nucleic Acids Res* (1998) 26:497–504. doi: 10.1093/nar/26.2.497

8. Hatziapostolou M, Polytarchou C, Aggelidou E, Drakaki A, Poultsides GA, Jaeger SA, et al. An HNF4α-miRNA inflammatory feedback circuit regulates hepatocellular oncogenesis. *Cell* (2011) 147:1233–47. doi: 10.1016/j.cell.2011.10.043

9. Walesky C, Apte U. Role of hepatocyte nuclear factor 4α (HNF4α) in cell proliferation and cancer. *Gene Expr* (2015) 16:101–8. doi: 10.3727/105221615X14181438356292

10. Ning B-F, Ding J, Yin C, Zhong W, Wu K, Zeng X, et al. Hepatocyte nuclear factor 4 alpha suppresses the development of hepatocellular carcinoma. *Cancer Res* (2010) 70:7640–51. doi: 10.1158/0008-5472.CAN-10-0824

11. Tanaka T, Jiang S, Hotta H, Takano K, Iwanari H, Sumi K, et al. Dysregulated expression of P1 and P2 promoter-driven hepatocyte nuclear factor-4alpha in the pathogenesis of human cancer. *J Pathol* (2006) 208:662–72. doi: 10.1002/path.1928

12. Fekry B, Ribas-Latre A, Baumgartner C, Deans JR, Kwok C, Patel P, et al. Incompatibility of the circadian protein BMAL1 and HNF4α in hepatocellular carcinoma. *Nat Commun* (2018) 9:4349. doi: 10.1038/s41467-018-06648-6

13. Cai S-H, Lu S-X, Liu L-L, Zhang CZ, Yun J-P. Increased expression of hepatocyte nuclear factor 4 alpha transcribed by promoter 2 indicates a poor prognosis in hepatocellular carcinoma. *Therap Adv Gastroenterol* (2017) 10:761–71. doi: 10.1177/1756283X17725998

14. Damiola F, Le Minh N, Preitner N, Kornmann B, Fleury-Olela F, Schibler U. Restricted feeding uncouples circadian oscillators in peripheral tissues from the central pacemaker in the suprachiasmatic nucleus. *Genes Dev* (2000) 14:2950–61. doi: 10.1101/gad.183500

15. Greco CM, Koronowski KB, Smith JG, Shi J, Kunderfranco P, Carriero R, et al. Integration of feeding behavior by the liver circadian clock reveals network dependency of metabolic rhythms. *Sci Adv* (2021) 7:eabi7828. doi: 10.1126/sciadv.abi7828

16. Dyar KA, Lutter D, Artati A, Ceglia NJ, Liu Y, Armenta D, et al. Atlas of circadian metabolism reveals system-wide coordination and communication between clocks. *Cell* (2018) 174:1571–1585.e11. doi: 10.1016/j.cell.2018.08.042

17. Gnocchi D, Pedrelli M, Hurt-Camejo E, Parini P. Lipids around the clock: focus on circadian rhythms and lipid metabolism. *Biology* (2015) 4:104–32. doi: 10.3390/biology4010104

18. Gnocchi D, Custodero C, Sabbà C, Mazzocca A. Circadian rhythms: a possible new player in non-alcoholic fatty liver disease pathophysiology. *J Mol Med* (2019) 97:741–59. doi: 10.1007/s00109-019-01780-2

19. Gnocchi D, Bruscalupi G. Circadian rhythms and hormonal homeostasis: pathophysiological implications. *Biology* (2017) 6. doi: 10.3390/biology6010010

20. Li Da, Cao T, Sun X, Jin S, Xie Di, Huang X, et al. Hepatic TET3 contributes to type-2 diabetes by inducing the HNF4α fetal isoform. *Nat Commun* (2020) 11:342. doi: 10.1038/s41467-019-14185-z

21. Kettner NM, Voicu H, Finegold MJ, Coarfa C, Sreekumar A, Putluri N, et al. Circadian homeostasis of liver metabolism suppresses hepatocarcinogenesis. *Cancer Cell* (2016) 30:909–24. doi: 10.1016/j.ccell.2016.10.007

22. Jouffe C, Weger BD, Martin E, Atger F, Weger M, Gobet C, et al. Disruption of the circadian clock component BMAL1 elicits an endocrine adaption impacting on insulin sensitivity and liver disease. *Proc Natl Acad Sci USA* (2022) 119:e2200083119. doi: 10.1073/pnas.2200083119

23. Briançon N, Weiss MC. *In vivo* role of the HNF4α AF-1 activation domain revealed by exon swapping. *EMBO J* (2006) 25:1253–62. doi: 10.1038/sj.emboj.7601021

24. Halkes CJM, van Dijk H, Verseyden C, de Jaegere PPT, Plokker HWM, Meijssen S, et al. Gender differences in postprandial ketone bodies in normolipidemic subjects and in untreated patients with familial combined hyperlipidemia. *Arterioscler Thromb Vasc Biol* (2003) 23:1875–80. doi: 10.1161/01.ATV.0000092326.00725.ED

25. Pervouchine DD, Djebali S, Breschi A, Davis CA, Barja PP, Dobin A, et al. Enhanced transcriptome maps from multiple mouse tissues reveal evolutionary constraint in gene expression. *Nat Commun* (2015) 6:5903. doi: 10.1038/ncomms6903

26. Walesky C, Gunewardena S, Terwilliger EF, Edwards G, Borude P, Apte U. Hepatocyte-specific deletion of hepatocyte nuclear factor-4α in adult mice results in increased hepatocyte proliferation. *Am J Physiol Gastrointest Liver Physiol* (2013) 304:G26–37. doi: 10.1152/ajpgi.00064.2012

27. Zhao X, Cho H, Yu RT, Atkins AR, Downes M, Evans RM. Nuclear receptors rock around the clock. *EMBO Rep* (2014) 15:518–28. doi: 10.1002/embr.201338271

28. Tahara Y, Shibata S. Circadian rhythms of liver physiology and disease: experimental and clinical evidence. *Nat Rev Gastroenterol Hepatol* (2016) 13:217–26. doi: 10.1038/nrgastro.2016.8

29. Qu M, Duffy T, Hirota T, Kay SA. Nuclear receptor HNF4A transrepresses CLOCK : BMAL1 and modulates tissue-specific circadian networks. *Proc Natl Acad Sci U.S.A.* (2018) 115:E12305–12. doi: 10.1073/pnas.1816411115

30. Qu M, Qu H, Jia Z, Kay SA. HNF4A defines tissue-specific circadian rhythms by beaconing BMAL1::CLOCK chromatin binding and shaping the rhythmic chromatin landscape. *Nat Commun* (2021) 12:6350. doi: 10.1038/s41467-021-26567-3

31. Torres-Padilla ME, Sladek FM, Weiss MC. Developmentally regulated N-terminal variants of the nuclear receptor hepatocyte nuclear factor 4alpha mediate multiple interactions through coactivator and corepressor-histone deacetylase complexes. *J Biol Chem* (2002) 277:44677–87. doi: 10.1074/jbc.M207545200

32. Bolotin E, Chellappa K, Hwang-Verslues W, Schnabl JM, Yang C, Sladek FM. Nuclear receptor HNF4a binding sequences are widespread in alu repeats. *BMC Genomics* (2011) 12:560. doi: 10.1186/1471-2164-12-560

33. Oshida K, Vasani N, Waxman DJ, Corton JC. Disruption of STAT5b-regulated sexual dimorphism of the liver transcriptome by diverse factors is a common event. *PloS One* (2016) 11:e0148308. doi: 10.1371/journal.pone.0148308

34. Clodfelter KH, Miles GD, Wauthier V, Holloway MG, Zhang X, Hodor P, et al. Role of STAT5a in regulation of sex-specific gene expression in female but not male mouse liver revealed by microarray analysis. *Physiol Genomics* (2007) 31:63–74. doi: 10.1152/physiolgenomics.00055.2007

35. Hwang-Verslues WW, Sladek FM. HNF4α–role in drug metabolism and potential drug target? *Curr Opin Pharmacol* (2010) 10:698–705. doi: 10.1016/j.coph.2010.08.010

36. Hirao J, Nishimura M, Arakawa S, Niino N, Mori K, Furukawa T, et al. Sex and circadian modulatory effects on rat liver as assessed by transcriptome analyses. *J Toxicol Sci* (2011) 36:9–22. doi: 10.2131/jts.36.9

37. Yuan X, Ta TC, Lin M, Evans JR, Dong Y, Bolotin E, et al. Identification of an endogenous ligand bound to a native orphan nuclear receptor. *PloS One* (2009) 4:e5609. doi: 10.1371/journal.pone.0005609

38. Tolson AH, Wang H. Regulation of drug-metabolizing enzymes by xenobiotic receptors: PXR and CAR. *Adv Drug Deliv Rev* (2010) 62:1238–49. doi: 10.1016/j.addr.2010.08.006

39. Kamiya A, Inoue Y, Gonzalez FJ. Role of the hepatocyte nuclear factor 4alpha in control of the pregnane X receptor during fetal liver development. *Hepatology* (2003) 37:1375–84. doi: 10.1053/jhep.2003.50212

40. Wagner K, Inceoglu B, Hammock BD. Soluble epoxide hydrolase inhibition, epoxygenated fatty acids and nociception. *Prostaglandins Other Lipid Mediat* (2011) 96:76–83. doi: 10.1016/j.prostaglandins.2011.08.001

41. Conforto TL, Waxman DJ. Sex-specific mouse liver gene expression: genome-wide analysis of developmental changes from pre-pubertal period to young adulthood. *Biol Sex Differ* (2012) 3:9. doi: 10.1186/2042-6410-3-9

42. Wiwi CA, Gupte M, Waxman DJ. Sexually dimorphic P450 gene expression in liver-specific hepatocyte nuclear factor 4alpha-deficient mice. *Mol Endocrinol* (2004) 18:1975–87. doi: 10.1210/me.2004-0129

43. Huang A, Sun D. Sexually dimorphic regulation of EET synthesis and metabolism: roles of estrogen. *Front Pharmacol* (2018) 9:1222. doi: 10.3389/fphar.2018.01222

44. Kardassis D, Falvey E, Tsantili P, Hadzopoulou-Cladaras M, Zannis V. Direct physical interactions between HNF-4 and Sp1 mediate synergistic transactivation of the apolipoprotein CIII promoter. *Biochemistry* (2002) 41:1217–28. doi: 10.1021/bi015618f

45. Hwang-Verslues WW, Sladek FM. Nuclear receptor hepatocyte nuclear factor 4alpha1 competes with oncoprotein c-Myc for control of the p21/WAF1 promoter. *Mol Endocrinol* (2008) 22:78–90. doi: 10.1210/me.2007-0298

46. Takahashi S, Matsuura N, Kurokawa T, Takahashi Y, Miura T. Co-operation of the transcription factor hepatocyte nuclear factor-4 with Sp1 or Sp3 leads to transcriptional activation of the human haem oxygenase-1 gene promoter in a hepatoma cell line. *Biochem J* (2002) 367:641–52. doi: 10.1042/bj20020819

47. Hall RK, Sladek FM, Granner DK. The orphan receptors COUP-TF and HNF-4 serve as accessory factors required for induction of phosphoenolpyruvate carboxykinase gene transcription by glucocorticoids. *Proc Natl Acad Sci USA* (1995) 92:412–6. doi: 10.1073/pnas.92.2.412

48. Lee YK, Dell H, Dowhan DH, Hadzopoulou-Cladaras M, Moore DD. The orphan nuclear receptor SHP inhibits hepatocyte nuclear factor 4 and retinoid X receptor transactivation: two mechanisms for repression. *Mol Cell Biol* (2000) 20:187–95. doi: 10.1128/MCB.20.1.187-195.2000

49. Hernandez JP, Chapman LM, Kretschmer XC, Baldwin WS. Gender-specific induction of cytochrome P450s in nonylphenol-treated FVB/NJ mice. *Toxicol Appl Pharmacol* (2006) 216:186–96. doi: 10.1016/j.taap.2006.05.014

50. Hock MB, Kralli A. Transcriptional control of mitochondrial biogenesis and function. *Annu Rev Physiol* (2009) 71:177–203. doi: 10.1146/annurev.physiol.010908.163119

51. Sladek FM, Ruse MDJr, Nepomuceno L, Huang SM, Stallcup MR. Modulation of transcriptional activation and coactivator interaction by a splicing variation in the F domain of nuclear receptor hepatocyte nuclear factor 4alpha1. *Mol Cell Biol* (1999) 19:6509–22. doi: 10.1128/MCB.19.10.6509

52. Maeda Y, Rachez C, Hawel L 3rd, Byus CV, Freedman LP, Sladek FM. Polyamines modulate the interaction between nuclear receptors and vitamin D receptor-interacting protein 205. *Mol Endocrinol* (2002) 16:1502–10. doi: 10.1210/mend.16.7.0883

53. Ruse MD Jr, Privalsky ML, Sladek FM. Competitive cofactor recruitment by orphan receptor hepatocyte nuclear factor 4alpha1: modulation by the F domain. *Mol Cell Biol* (2002) 22:1626–38. doi: 10.1128/MCB.22.6.1626-1638.2002

54. Ikaga R, Namekata I, Kotiadis VN, Ogawa H, Duchen MR, Tanaka H, et al. Knockdown of aquaporin-8 induces mitochondrial dysfunction in 3T3-L1 cells. *Biochem Biophys Rep* (2015) 4:187–95. doi: 10.1016/j.bbrep.2015.09.009

55. Eckel-Mahan KL, Patel VR, de Mateo S, Orozco-Solis R, Ceglia NJ, Sahar S, et al. Reprogramming of the circadian clock by nutritional challenge. *Cell* (2013) 155:1464–78. doi: 10.1016/j.cell.2013.11.034

56. Ribas-Latre A, Eckel-Mahan K. Interdependence of nutrient metabolism and the circadian clock system: Importance for metabolic health. *Mol Metab* (2016) 5:133–52. doi: 10.1016/j.molmet.2015.12.006

57. Eckel-Mahan KL, Patel VR, Mohney RP, Vignola KS, Baldi P, Sassone-Corsi P. Coordination of the transcriptome and metabolome by the circadian clock. *Proc Natl Acad Sci USA* (2012) 109:5541–6. doi: 10.1073/pnas.1118726109

58. Marinou K, Adiels M, Hodson L, Frayn KN, Karpe F, Fielding BA. Young women partition fatty acids towards ketone body production rather than VLDL-TAG synthesis, compared with young men. *Br J Nutr* (2011) 105:857–65. doi: 10.1017/S0007114510004472

59. Puchalska P, Crawford PA. Multi-dimensional roles of ketone bodies in fuel metabolism, signaling, and therapeutics. *Cell Metab* (2017) 25:262–84. doi: 10.1016/j.cmet.2016.12.022

60. Chavan R, Feillet C, Costa SSF, Delorme JE, Okabe T, Ripperger JA, et al. Liver-derived ketone bodies are necessary for food anticipation. *Nat Commun* (2016) 7:10580. doi: 10.1038/ncomms10580

61. Holloway MG, Miles GD, Dombkowski AA, Waxman DJ. Liver-specific hepatocyte nuclear factor-4alpha deficiency: greater impact on gene expression in male than in female mouse liver. *Mol Endocrinol* (2008) 22:1274–86. doi: 10.1210/me.2007-0564

62. Nassir F, Ibdah JA. Sirtuins and nonalcoholic fatty liver disease. *World J Gastroenterol* (2016) 22:10084–92. doi: 10.3748/wjg.v22.i46.10084

63. Rodríguez JC, Ortiz JA, Hegardt FG, Haro D. The hepatocyte nuclear factor 4 (HNF-4) represses the mitochondrial HMG-CoA synthase gene. *Biochem Biophys Res Commun* (1998) 242:692–6. doi: 10.1006/bbrc.1997.8032

64. Tognini P, Murakami M, Liu Y, Eckel-Mahan KL, Newman JC, Verdin E, et al. Distinct circadian signatures in liver and gut clocks revealed by ketogenic diet. *Cell Metab* (2017) 26:523–538.e5. doi: 10.1016/j.cmet.2017.08.015

65. Rando G, Tan CK, Khaled N, Montagner A, Leuenberger N, Bertrand-Michel J, et al. Glucocorticoid receptor-PPARα axis in fetal mouse liver prepares neonates for milk lipid catabolism. *Elife* (2016) 5. doi: 10.7554/eLife.11853

66. Bailly A, Briançon N, Weiss MC. Characterization of glucocorticoid receptor and hepatocyte nuclear factor 4alpha (HNF4alpha) binding to the hnf4alpha gene in the liver. *Biochimie* (2009) 91:1095–103. doi: 10.1016/j.biochi.2009.06.009

67. Robles MS, Cox J, Mann M. *In-vivo* quantitative proteomics reveals a key contribution of post-transcriptional mechanisms to the circadian regulation of liver metabolism. *PloS Genet* (2014) 10:e1004047. doi: 10.1371/journal.pgen.1004047

68. Argemi J, Latasa MU, Atkinson SR, Blokhin IO, Massey V, Gue JP, et al. Defective HNF4alpha-dependent gene expression as a driver of hepatocellular failure in alcoholic hepatitis. *Nat Commun* (2019) 10:3126. doi: 10.1038/s41467-019-11004-3

69. Lu Y, Li N, Gao L, Xu Y-J, Huang C, Yu K, et al. Acetylcarnitine is a candidate diagnostic and prognostic biomarker of hepatocellular carcinoma. *Cancer Res* (2016) 76:2912–20. doi: 10.1158/0008-5472.CAN-15-3199

70. Yaligar J, Teoh WW, Othman R, Verma SK, Phang BH, Lee SS, et al. Longitudinal metabolic imaging of hepatocellular carcinoma in transgenic mouse models identifies acylcarnitine as a potential biomarker for early detection. *Sci Rep* (2016) 6:20299. doi: 10.1038/srep20299

71. Gnocchi D, Sabbà C, Massimi M, Mazzocca A. Metabolism as a new avenue for hepatocellular carcinoma therapy. *Int J Mol Sci* (2023) 24(4):3710. doi: 10.3390/ijms24043710

72. Kolb H, Kempf K, Röhling M, Lenzen-Schulte M, Schloot NC, Martin S. Ketone bodies: from enemy to friend and guardian angel. *BMC Med* (2021) 19:313. doi: 10.1186/s12916-021-02185-0

73. Chen T-Y, Li Y-C, Liu Y-F, Tsai C-M, Hsieh Y-H, Lin C-W, et al. Role of MMP14 gene polymorphisms in susceptibility and pathological development to hepatocellular carcinoma. *Ann Surg Oncol* (2011) 18:2348–56. doi: 10.1245/s10434-011-1574-x

74. Zheng S, Wu H, Wang F, Lv J, Lu J, Fang Q, et al. The oncoprotein HBXIP facilitates metastasis of hepatocellular carcinoma cells by activation of MMP15 expression. *Cancer Manag Res* (2019) 11:4529–40. doi: 10.2147/CMAR.S198783

75. Chen Z, Wu G, Ye F, Chen G, Fan Q, Dong H, et al. High expression of MMP19 is associated with poor prognosis in patients with colorectal cancer. *BMC Cancer* (2019) 19:448. doi: 10.1186/s12885-019-5673-6

76. Delbès A-S, Quiñones M, Gobet C, Castel J, Denis RGP, Berthelet J, et al. Mice with humanized livers reveal the role of hepatocyte clocks in rhythmic behavior. *Sci Adv* (2023) 9:eadf2982. doi: 10.1126/sciadv.adf2982

77. Yan J, Chen B, Lu J, Xie W. Deciphering the roles of the constitutive androstane receptor in energy metabolism. *Acta Pharmacol Sin* (2015) 36:62–70. doi: 10.1038/aps.2014.102

78. Debruyne JP, Noton E, Lambert CM, Maywood ES, Weaver DR, Reppert SM. A clock shock: mouse CLOCK is not required for circadian oscillator function. *Neuron* (2006) 50:465–77. doi: 10.1016/j.neuron.2006.03.041

79. Vuong LM, Chellappa K, Dhahbi JM, Deans JR, Fang B, Bolotin E, et al. Differential effects of hepatocyte nuclear factor 4α Isoforms on tumor growth and T-cell factor 4/AP-1 interactions in human colorectal cancer cells. *Mol Cell Biol* (2015) 35:3471–90. doi: 10.1128/MCB.00030-15

80. Risso D, Schwartz K, Sherlock G, Dudoit S. GC-content normalization for RNA-Seq data. *BMC Bioinf* (2011) 12:480. doi: 10.1186/1471-2105-12-480

81. Stark R, Brown G. *DiffBind: differential binding analysis of ChIP-Seq peak data* Vol. 100. R package version (2011). Available at: https://www.anjoumacpherson.com/packages/2.13/bioc/vignettes/DiffBind/inst/doc/DiffBind.pdf.

82. Bolotin E, Liao H, Ta TC, Yang C, Hwang-Verslues W, Evans JR, et al. Integrated approach for the identification of human hepatocyte nuclear factor 4alpha target genes using protein binding microarrays. *Hepatology* (2010) 51:642–53. doi: 10.1002/hep.23357

83. Jiang G, Nepomuceno L, Hopkins K, Sladek FM. Exclusive homodimerization of the orphan receptor hepatocyte nuclear factor 4 defines a new subclass of nuclear receptors. *Mol Cell Biol* (1995) 15:5131–43. doi: 10.1128/MCB.15.9.5131

84. Verzi MP, Shin H, He HH, Sulahian R, Meyer CA, Montgomery RK, et al. Differentiation-specific histone modifications reveal dynamic chromatin interactions and partners for the intestinal transcription factor CDX2. *Dev Cell* (2010) 19:713–26. doi: 10.1016/j.devcel.2010.10.006

85. Mohammed H, Taylor C, Brown GD, Papachristou EK, Carroll JS, D'Santos CS. Rapid immunoprecipitation mass spectrometry of endogenous proteins (RIME) for analysis of chromatin complexes. *Nat Protoc* (2016) 11:316–26. doi: 10.1038/nprot.2016.020

86. Deol P, Fahrmann J, Yang J, Evans JR, Rizo A, Grapov D, et al. Omega-6 and omega-3 oxylipins are implicated in soybean oil-induced obesity in mice. *Sci Rep* (2017) 7:12488. doi: 10.1038/s41598-017-12624-9

87. *West coast metabolomics center - assays and services*. Available at: https://metabolomics.ucdavis.edu/core-services/assays-and-services (Accessed October 8, 2023).

88. Xia J, Wishart DS. Using metaboAnalyst 3.0 for comprehensive metabolomics data analysis. In: *Current protocols in bioinformatics*. (Hoboken, NJ: John Wiley & Sons, Inc) (2002).

89. Yang J, Schmelzer K, Georgi K, Hammock BD. Quantitative profiling method for oxylipin metabolome by liquid chromatography electrospray ionization tandem mass spectrometry. *Anal Chem* (2009) 81:8085–93. doi: 10.1021/ac901282n

90. Matyash V, Liebisch G, Kurzchalia TV, Shevchenko A, Schwudke D. Lipid extraction by methyl-tert-butyl ether for high-throughput lipidomics. *J Lipid Res* (2008) 49:1137–46. doi: 10.1194/jlr.D700041-JLR200